

# Spectroscopic search for new SW Sextantis stars in the 3–4 hour orbital period range – I.

P. Rodríguez-Gil<sup>1,2\*</sup>, L. Schmidtobreick<sup>2</sup> and B. T. Gänsicke<sup>3</sup>

<sup>1</sup>*Instituto de Astrofísica de Canarias, Vía Láctea s/n, La Laguna, E-38205, Santa Cruz de Tenerife, Spain*

<sup>2</sup>*European Southern Observatory, Casilla 19001, Santiago 19, Chile*

<sup>3</sup>*Department of Physics, University of Warwick, Coventry CV4 7AL, UK*

Accepted 2006. Received 2006

## ABSTRACT

We report on time-resolved optical spectroscopy of ten non-eclipsing nova-like cataclysmic variables in the orbital period range between 3 and 4 hours. The main objective of this long-term programme is to search for the characteristic SW Sextantis behaviour and to eventually quantify the impact of the SW Sex phenomenon on nova-likes at the upper boundary of the orbital period gap.

Of the ten systems so far observed, HL Aqr, BO Cet, AH Men, V380 Oph, AH Pic, and LN UMa are identified as new members of the SW Sex class. We present improved orbital period measurements for HL Aqr ( $P_{\text{orb}} = 3.254 \pm 0.001$  h) and V380 Oph ( $P_{\text{orb}} = 3.69857 \pm 0.00002$  h). BO Cet and V380 Oph exhibit emission-line flaring with periodicities of 20 min and 47 min, respectively. The H $\alpha$  line of HL Aqr shows significant blueshifted absorption modulated at the orbital period. Similarly to the emission S-wave of the high-inclination SW Sex stars, this *absorption* S-wave has its maximum blue velocity at orbital phase  $\sim 0.5$ . We estimate an orbital inclination for HL Aqr in the range  $19^\circ < i < 27^\circ$ , which is much lower than that of the emission-dominated, non-eclipsing SW Sex stars ( $i \sim 60^\circ - 70^\circ$ ). This gives rise to the interesting possibility of many low-inclination nova-likes actually being SW Sex stars, but with a very different spectroscopic appearance as they show significant absorption. The increasing blueshifted absorption with decreasing inclination points to the existence of a mass outflow with significant vertical motion.

This six new additions to the SW Sex class increase the presence of non-eclipsing systems to about one third of the whole SW Sex population, which therefore makes the requirement of eclipses as a defining criterion for SW Sex membership no longer valid. The statistics of the cataclysmic variable population in the vicinity of the upper period gap is also discussed.

**Key words:** accretion, accretion discs – binaries: close – stars: individual: HL Aqr, BO Cet, V849 Her, V393 Hya, AH Men, V380 Oph, LQ Peg, AH Pic, V992 Sco, LN UMa – novae, cataclysmic variables

## 1 INTRODUCTION

The theory of cataclysmic variable (CV) evolution predicts an abrupt cessation of mass transfer at an orbital period of  $\sim 3$  h, i.e. the upper boundary of the period gap, where magnetic braking is believed to be interrupted. However, it is becoming increasingly clear that the upper edge of the gap is overpopulated by CVs which show unusual behaviour. These systems, collectively known as the SW Sextantis stars (Thorstensen et al. 1991), show a number of common properties, including uncommon “V”-shaped eclipse profiles, the

presence of He II  $\lambda 4686$  emission, substantial delays of the radial velocities of the Balmer and He I lines with respect to the motion of the white dwarf, single-peaked emission lines that display central absorption dips around orbital phases  $\simeq 0.4 - 0.7$ , and high-velocity emission S-waves with maximum blueshift near phase  $\sim 0.5$ . These observational characteristics do not easily fit into the picture of a steady-state, hot optically-thick accretion disc which is expected to be common in intrinsically bright, weakly-magnetic CVs above the period gap.

In terms of numbers, the SW Sex stars currently represent half the total population of nova-likes in the 3 – 4 h orbital period range (Rodríguez-Gil 2005, Aungwerojwit et al.

\* E-mail: prguez@iac.es

2005, Rodríguez-Gil et al. 2007). Thus, their study is of critical importance to investigate the evolution of CVs as they enter the gap.

Many different ideas have been proposed to model the unusual behaviour of the SW Sex stars, but none of them has been able to explain the SW Sex phenomenon in full. Among the many mechanisms so far invoked we highlight stream overflow (Hellier & Robinson 1994; Hellier 1996), magnetic accretion (Rodríguez-Gil et al. 2001; Hameury & Lasota 2002), magnetic propeller anchored in the inner disc (Horne 1999), and self-obscuraton of the inner disc by a flared outer disc (Knigge et al. 2000).

In order to address the actual impact of the SW Sex phenomenon on the nova-like population found between 3 and 4 hours, we started to search for characteristic SW Sex features in poorly-studied nova-likes of both hemispheres in that period range. Since the majority of these properties are actually spectroscopic we will entirely focus on phase-resolved optical spectroscopy. This paper contains the first results of this project.

## 2 OBSERVATIONAL DATA AND THEIR REDUCTION

Time-resolved spectroscopy of the candidate SW Sex stars was carried out with the New Technology Telescope (NTT) at the European Southern Observatory on La Silla, and the William Herschel Telescope (WHT) at the Roque de los Muchachos Observatory on La Palma. At the NTT the EMMI (ESO Multi-Mode Instrument) was used in the Medium Dispersion Spectroscopy mode with grating D/7 centered on  $H\alpha$  and the  $2048 \times 4096$  pixel<sup>2</sup> MIT/LL CCD detector. A useful wavelength range of  $\lambda\lambda 6170 - 6900$  at  $0.8 \text{ \AA}$  spectral resolution (full width at half maximum, FWHM) was obtained with a  $1.0$ -arcsec slit width.

The double-armed ISIS spectrograph was used to perform the observations at the WHT. The blue and red arms were equipped with the R600B and the R316R gratings, respectively. The wavelength ranges  $\lambda\lambda 3700 - 5045$  and  $\lambda\lambda 6230 - 8900$  were sampled at  $1.8 \text{ \AA}$  and  $3.3 \text{ \AA}$  resolution (FWHM;  $1.0$ -arcsec slit) on the  $2048 \times 4200$  pixel<sup>2</sup> EEV12 and the  $2148 \times 4700$  pixel<sup>2</sup> Marconi CCDs in the blue and the red, respectively. Spectra of arc lamps were regularly taken in order to achieve a proper wavelength calibration in both telescopes. See Table 1 for some details of the observations.

The spectroscopic data were reduced using standard procedures in IRAF<sup>1</sup>. After subtracting the bias level, the images were divided by an average flat field which was normalised by fitting Chebyshev functions to remove the detector specific spectral response. The sky contribution was then subtracted and the final spectra optimally extracted following the method described by Horne (1986). For wavelength calibration, a low-order polynomial was fitted to the pixel-wavelength arc data. The wavelength solution for each target spectrum was obtained by interpolating between the

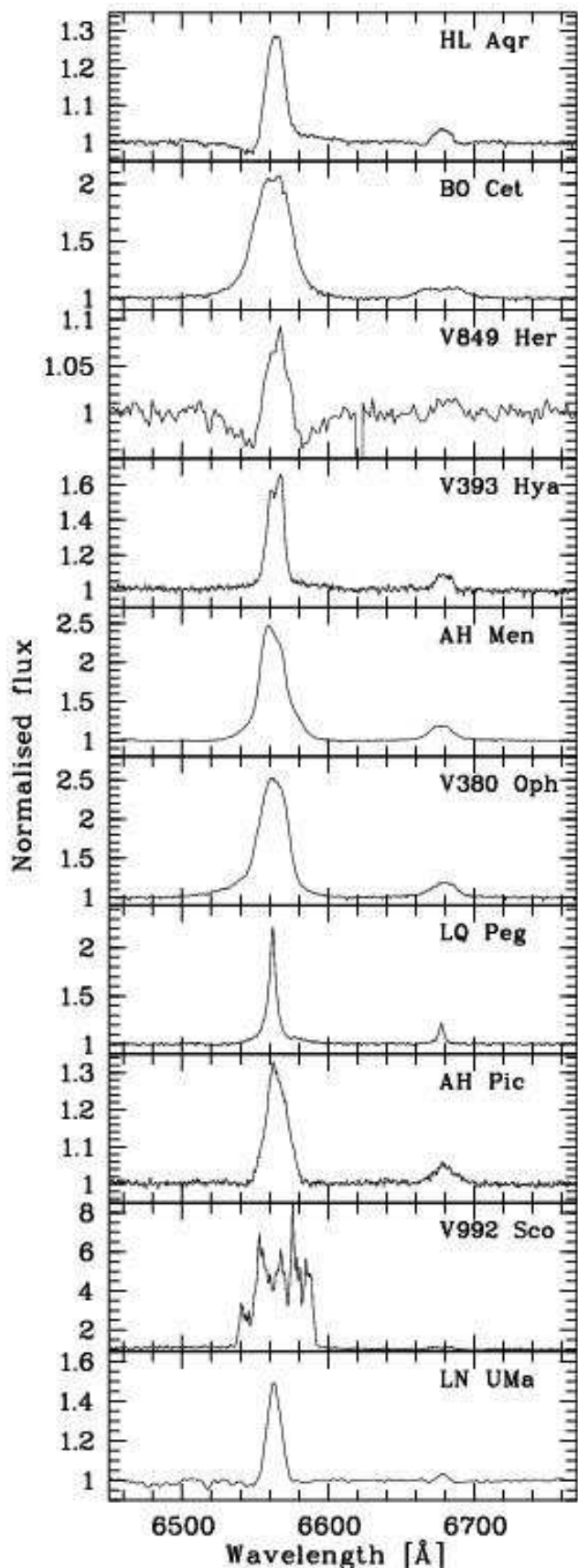


**Figure 1.** Average spectra around  $H\alpha$  of all the SW Sex candidates observed. The continuum has been normalised to unity.

<sup>1</sup> IRAF is distributed by the National Optical Astronomy Observatories.

**Table 1.** Summary of the observational details. The object name, date and UT at the start of the first exposure, the number of exposures, the individual exposure time, and the covered orbital cycles are given (with the exception of LQ Peg, for which  $P_{\text{orb}}$  is not known).

Name	Date	UT	# <sub>exp</sub>	$t_{\text{exp}}$ [s]	Cycles
HL Aqr	2005-09-27	02:50:04	35	300	0.99
	2005-09-28	00:30:19	37	300	1.05
BO Cet	2005-09-27	06:25:17	36	300	0.99
V849 Her	2005-05-22	23:42:50	25 blue	300	0.84
	2005-05-22	23:42:50	25 red	300	0.84
V393 Hya	2005-04-17	03:07:02	6	600	0.28
	2005-04-18	03:15:44	15	600	0.80
AH Men	2005-04-16	23:21:24	18	600	1.14
V380 Oph	2005-04-17	06:05:33	16	900	1.08
	2005-05-23	04:09:56	12 blue	300	0.39
	2005-05-23	04:09:56	12 red	300	0.39
	2005-05-24	01:25:02	67 blue	180	1.03
	2005-05-24	01:25:02	67 red	180	1.03
LQ Peg	2005-09-26	23:32:40	17	600	—
AH Pic	2005-04-17	23:26:53	24	480	1.03
V992 Sco	2005-04-18	06:15:55	15	900	1.02
LN UMa	2005-05-23	21:13:30	39 blue	300	1.05
	2005-05-23	21:13:30	39 red	300	1.05

two nearest arc spectra. All subsequent analysis was done with the MOLLY<sup>2</sup> package.

### 3 CRITERIA FOR SW SEX STATUS

Before presenting the results on the individual objects it is worth clarifying which spectroscopic characteristics a nova-like must display in order to be classified as a SW Sex star. Note that not all the SW Sex stars show the whole set of features we will describe here at any one time.

The SW Sex class was initially populated by eclipsing systems only (Thorstensen et al. 1991). Contrary to what is expected for an accretion disc in Keplerian rotation viewed at high inclination, the emission lines observed in the SW Sex stars are single-peaked in both the eclipsing and non-eclipsing systems (compare e.g. the optical spectra of the dwarf nova HT Cas, Young et al. 1981, and the SW Sex star V1315 Aql, Dhillon et al. 1991). Significant He II  $\lambda 4686$  and Bowen blend emission are also typical of the SW Sex stars. Apart from that, the Balmer line profiles are highly asymmetric with enhanced wings extending up to  $\sim \pm 2000 - 3000 \text{ km s}^{-1}$ . The trailed spectra reveal that this is the consequence of a high-velocity emission S-wave which has maximum blue velocity at orbital phase  $\sim 0.5$  (see e.g. Casares et al. 1996, Hellier 2000, and Rodríguez-Gil et al. 2004). In addition, an absorption component in the Balmer and He I lines shows its maximum strength at the same orbital phase, transiently turning the single-peaked line profiles into “fake” double peaks (see Szkody & Piché 1990, Hellier 1996, and Hoard & Szkody 1997). However, the He II  $\lambda 4686$  emission line is not affected by this absorption. In the eclipsing SW Sex stars, the Balmer

and He I radial velocity curves (and occasionally He II  $\lambda 4686$ ) make their red to the blue crossing about 0.1 – 0.2 orbital cycle *later* than the phase zero defined by the eclipses (e.g. Hoard & Szkody 1997; Rodríguez-Gil et al. 2001). The same phase delays have been observed in non-eclipsing SW Sex stars, but in this case between the He II  $\lambda 4686$  (believed to follow the white dwarf motion) and the Balmer (and He I) radial velocity curves. As mentioned earlier, the He II  $\lambda 4686$  radial velocity curve occasionally shares the Balmer and He I phasing. When this happens, absolute phases are usually estimated by assuming that (i) the maximum blueshift of the high-velocity S-wave occurs at orbital phase  $\sim 0.5$ , or (ii) the strength of the transient absorption component is maximum also at that orbital phase (e.g. Thorstensen & Taylor 2000, Thorstensen & Taylor 2001). A SW Sex nature is therefore very likely if the emission-line radial velocity curves of a given nova-like show a  $\sim 0.1 - 0.2$  orbital cycle delay with respect to that phase convention, as it is then clear that it behaves in the way eclipsing SW Sex stars do.

As more spectroscopic studies with better time resolution (few minutes) are becoming available, it is apparent that the emission lines of some SW Sex stars show rapid variability with time-scales of the order of tens of minutes (Smith et al. 1998; Rodríguez-Gil et al. 2001; Rodríguez-Gil & Martínez-Pais 2002; also see the results on BO Cet and V380 Oph in this paper). This, however, cannot yet be considered as a common feature of the class due to the scarcity of studies with adequate time resolution.

Even though the behaviour of the emission lines in the SW Sex stars is a challenge for Doppler tomography techniques (eclipses, transient absorption, variability; see e.g. Steeghs 2003), the Doppler maps consistently share a common feature: the bulk of Balmer emission is concentrated in the  $(-V_x, -V_y)$  quadrant (e.g. Hellier & Robinson 1994; Hoard & Szkody 1997; Hoard et al. 2000; Rodríguez-Gil et al. 2001).

In summary, our SW Sex classification strategy can be outlined as follows:

- 1) First step will be to check whether the emission line profiles are single- or double-peaked in the average spectrum.
- 2) Check for the characteristic high-velocity, emission S-wave. Note that none of the systems presented in this paper shows eclipses. If no other component (as e.g. line emission from the irradiated donor star) can be used to determine absolute phases, we will assume that the maximum blue excursion of the S-wave takes place at phase  $\varphi \sim 0.5$  (see e.g. Hellier 1996; Hoard & Szkody 1997; Hellier 2000; Rodríguez-Gil et al. 2001), as it happens in the eclipsing SW Sex stars. To avoid confusion, we will use  $\varphi_r$  for relative phases and  $\varphi_a$  for (nearly) absolute phases. As a final note on phasing, the trailed spectrum diagrams and the folded radial velocity curves presented in the paper contain absolute phases unless otherwise stated.
- 3) Search for the transient absorption, which has to reach its maximum strength at phase  $\sim 0.5$  according to the above phase definition.
- 4) Check if the radial velocity curve of the line wings is delayed by 0.1 – 0.2 cycle. Unfortunately, most of our

<sup>2</sup> Tom Marsh’s MOLLY package is available at <http://deneb.astro.warwick.ac.uk/phsaap/software/>

**Table 2.** H $\alpha$  and He I  $\lambda$ 6678 FWHM and equivalent width (EW) for each system. The emission line parameters were measured in the average spectrum. No Gaussian fit was possible for H $\alpha$  in V992 Sco.

Name	H $\alpha$ FWHM [km s $^{-1}$ ]	He I $\lambda$ 6678 FWHM [km s $^{-1}$ ]	H $\alpha$ EW [Å]	He I $\lambda$ 6678 EW [Å]
HL Aqr	620	530	4.8(2)	0.4(2)
BO Cet	1310	1620	35.0(2)	3.5(2)
V393 Hya	580	520	9.6(3)	1.3(3)
AH Men	940	800	33.9(2)	4.3(2)
V380 Oph	1020	900	41.1(1)	4.4(1)
LQ Peg	310	210	10.3(1)	1.2(1)
AH Pic	760	780	5.5(1)	0.9(1)
V992 Sco	—	—	166.8(4)	2.6(3)
LN UMa	510	330	5.91(3)	0.3(2)

spectra only cover the H $\alpha$  and He I  $\lambda$ 6678 emission lines, thus phase lags with respect to the He II  $\lambda$ 4686 line cannot be investigated. This line is observed in three systems, for which blue WHT spectra were obtained (V849 Her, V380 Oph, and LN UMa), but it proved too weak to perform a radial velocity study in any of the systems.

5) Find the characteristic emission distribution in the Doppler tomogram.

#### 4 AVERAGE SPECTRA

In Fig. 1, the average spectra around H $\alpha$  for all observed SWSex candidates are plotted. All of them are dominated by H $\alpha$  in emission, with the exception of V849 Her which shows a broad absorption underneath the H $\alpha$  emission. Some blueshifted absorption is also observed in HL Aqr. Table 2 gives an overview on the width and strength of the H $\alpha$  and He I  $\lambda$ 6678 emission lines. The average H $\alpha$  lines do not show the double-peaked profiles characteristic of line emission in a Keplerian accretion disc. Only V393 Hya has a clear double-peaked profile. In what follows we will discuss the observed objects in detail.

### 5 RESULTS ON THE INDIVIDUAL OBJECTS

#### 5.1 HL Aqr

HL Aqr (= PHL 227; Haro & Luyten 1962) was identified as a CV by Hunger, Heber & Koester (1985), who classified it as a UX UMa nova-like according to its ultraviolet and optical spectra. Haefner & Schoembs (1987) showed that, despite the optical spectrum of HL Aqr exhibited broad H $\beta$  and H $\gamma$  absorptions with weak central emissions, the H $\alpha$  line was purely in emission. Their radial velocity analyses on this line yielded an orbital period of  $0.1356 \pm 0.0006$  d. In addition, they detected a coherent, low-amplitude oscillation in the *B*-band light curves at 19.6 s, which was later interpreted as a dwarf nova oscillation (DNO) by Warner (2004).

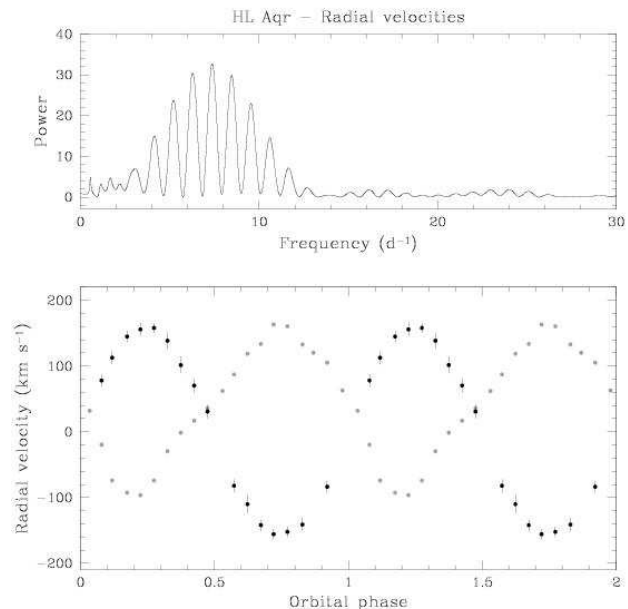


**Figure 2.** *Top:* Scargle periodogram computed from the H $\alpha$  radial velocity curve of HL Aqr obtained by cross-correlation with a double Gaussian template (700 km s $^{-1}$  separation, FWHM = 300 km s $^{-1}$ ). *Bottom:* the H $\alpha$  wings (gray) and donor emission velocities (black) folded on  $P_{\text{orb}} = 0.13557$  d and averaged into 20 phase bins. Four clearly deviating points have been excluded from the radial velocity curve of the donor star emission. The orbital cycle has been plotted twice.

#### 5.1.1 H $\alpha$ radial velocities and trailed spectrum

In our NTT spectra (Fig. 1) the H $\alpha$  line is almost entirely in emission but some absorption can be seen in the blue wing. The profile is single-peaked and has FWHM  $\simeq 620$  km s $^{-1}$  (Table 2). We computed the H $\alpha$  radial velocities by applying the double Gaussian technique of Schneider & Young (1980) using a 700 km s $^{-1}$  separation and FWHM = 300 km s $^{-1}$ . The Scargle periodogram (Scargle 1982) computed from the radial velocity data set (Fig. 2) provided an improved value of the orbital period of  $P = 0.13557 \pm 0.00005$  d ( $= 3.254 \pm 0.001$  h), where the quoted uncertainty comes from a sine fit to the radial velocity curves (Table 3). This value is in perfect agreement with the orbital period measured by Haefner & Schoembs (1987). The sine fit also provided a preliminary time of zero phase (i.e. velocity red-to-blue crossing) of  $T_0(\text{HJD}) = 2453640.75494 \pm 0.0003$ .

Relative orbital phases were computed by using the orbital period and the  $T_0$  measured from the radial velocities. The H $\alpha$  trailed spectrum (Fig. 3) of HL Aqr shows a narrow, low-amplitude S-wave with blue-to-red velocity crossing at  $\varphi_r = 0$ . This component is very likely coming from the (irradiated) donor star, which is supported by its maximum strength at  $\varphi_r = 0.5$ . Although not shown, the He I  $\lambda$ 6678 trailed spectrum also shows narrow emission from the secondary star. In order to obtain the actual  $T_0$  from the radial velocity curve of this emission, we proceeded as follows: the individual spectra were folded on the orbital period and averaged into 20 phase bins. A Gaussian-smoothed (FWHM = 200 km s $^{-1}$ ) version of each spectrum was then

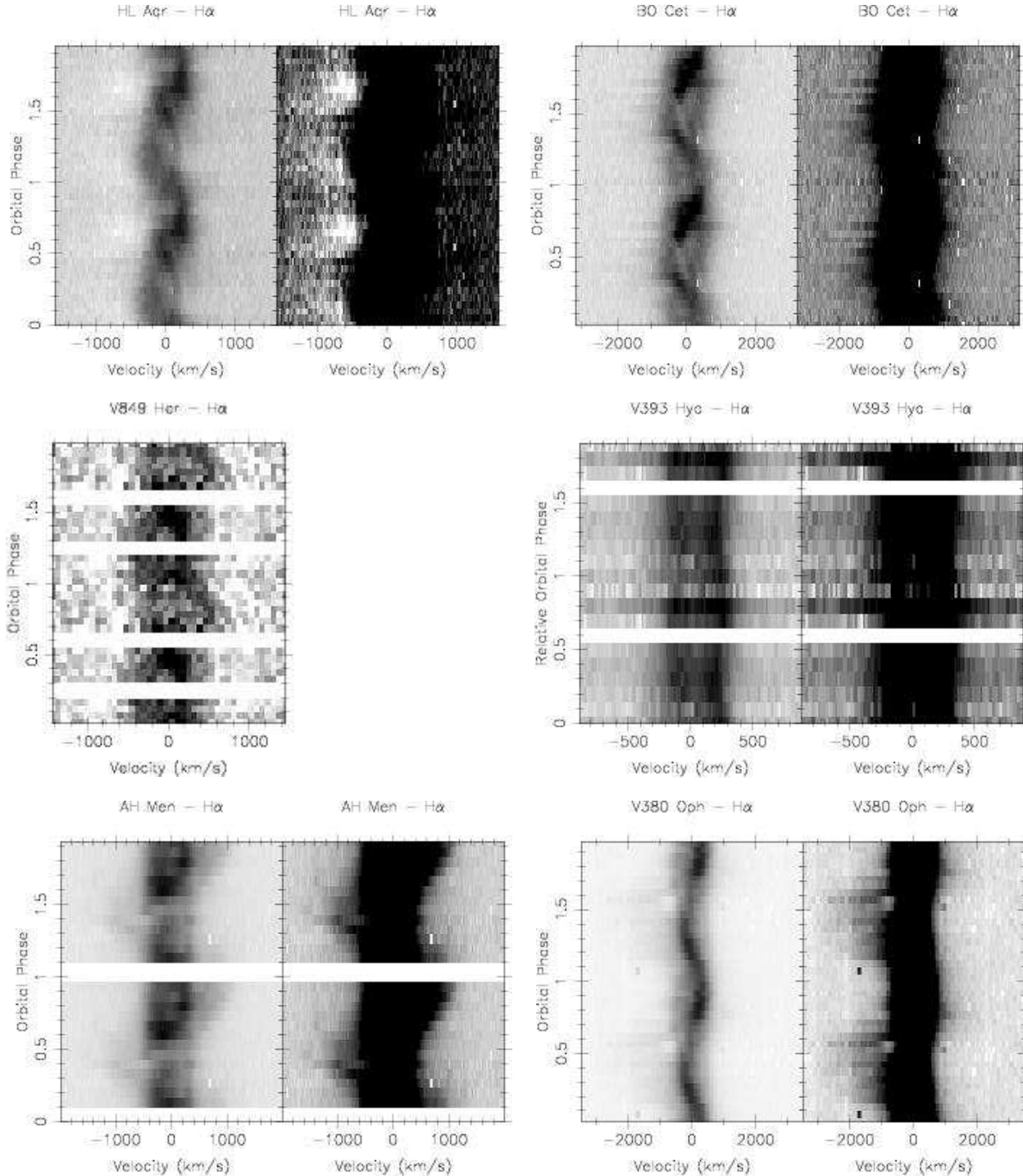


**Figure 3.**  $H\alpha$  trailed spectra. For each object (with the exception of V849 Her and V992 Sco) two panels with different contrast are shown. The left panel focuses on the line core whereas the right one emphasizes the wings.

subtracted from the actual one. A preliminary radial velocity curve was measured by means of a cursor on a new trailed spectrum, following by eye the path of the donor emission S-wave and clicking on its maximum flux for each phase bin. The spectra were subsequently applied a velocity shift according to that radial velocity curve in order to eliminate the velocity modulation of the donor emission, and were then averaged to construct an emission template which was centred on the rest velocity. A new radial velocity curve was finally

obtained by cross-correlation of the original phase-binned spectra with this template (Fig. 2). A sine fit to this phase-folded curve provided a negligible phase shift with respect to the preliminary  $T_0$ , which suggests that the radial velocities of the  $H\alpha$  wings are not delayed with respect to the motion of the white dwarf (final  $T_0$  values are given in Table 3). In contrast with the 0.1 – 0.2-cycle delays usually observed in the SW Sex stars, the radial velocity curve of the He I  $\lambda 6678$  line wings (not shown) *precedes* the white dwarf motion by

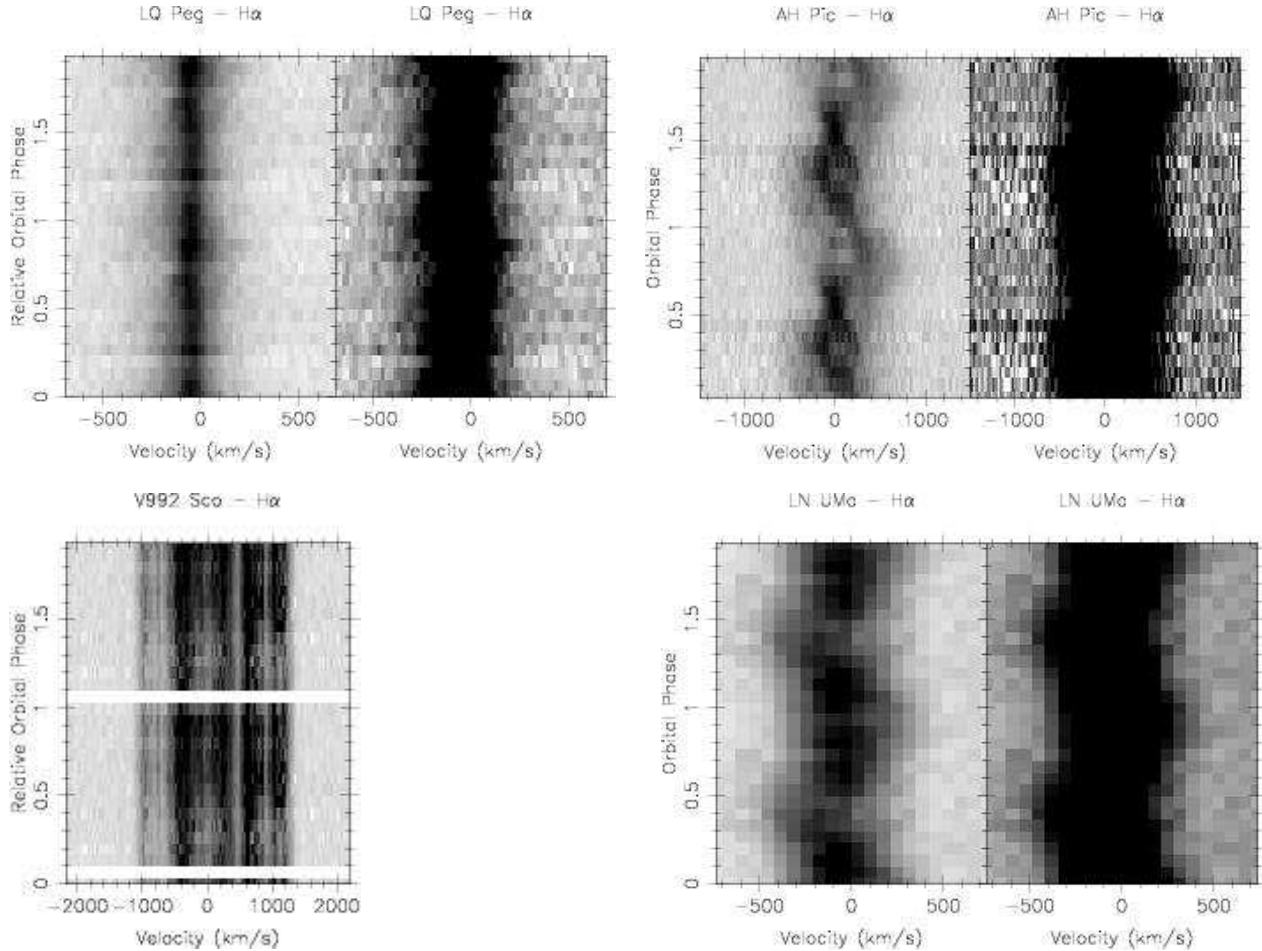


Figure 3. (cont.)

**Table 3.**  $H\alpha$  radial velocities sine fits parameters.  $T_0$  refers to the time of inferior conjunction of the secondary star.

Name	$P_{\text{orb}}$ [h]	$\gamma$ [km s $^{-1}$ ]	$K$ [km s $^{-1}$ ]	$T_0$ (HJD) [2453 400 +]
HL Aqr	3.254(1)	20(1) <sup>1</sup>	113(1)	240.7547(3) <sup>1</sup>
BO Cet	3.355(1)	-35(2) <sup>1</sup>	349(2)	240.7633(1) <sup>1</sup>
V849 Her	3.15(48)	-11(12) <sup>1</sup>	100(15)	313.536(5) <sup>1</sup>
V393 Hya	3.23	41(2)	46(3)	78.679(1)
AH Men	2.95	-11(1)	209(1)	77.5421(2) <sup>2</sup>
V380 Oph	3.69857(2)	11.7(4)	206.6(5)	114.61061(8) <sup>2</sup>
LQ Peg	2.80(2)	-55.4(2)	12.4(2)	240.5375(3) <sup>3</sup>
AH Pic	3.38(7)	32(2) <sup>1</sup>	94(5)	78.547(1) <sup>1</sup>
LN UMa	3.465(2)	-68(2)	62(2)	114.4461(9) <sup>2</sup>

<sup>1</sup>) From donor star emission.<sup>2</sup>) Corrected for phase delay.<sup>3</sup>) Uncertain.

0.1 orbital cycle. Note that the phasing and amplitude of the radial velocity curve of the donor's He I  $\lambda 6678$  emission (not shown) are the same as those of  $H\alpha$ .

The  $H\alpha$  trailed spectrum shows a dominant emission S-wave with maximum excursion to the blue at  $\varphi_a \simeq 0.3$ . No emission-line flaring is apparent. Remarkably, there is an absorption S-wave component blueshifted

by  $\sim 1000 \text{ km s}^{-1}$  with respect to the rest velocity which reaches maximum blue velocity at  $\varphi_a \simeq 0.5$ , that is, 0.3 cycle later than the  $H\alpha$  emission wings. This absorption may be indicative of a mass outflow in the system. The fact that it varies with the orbital period suggests that it may originate in a wind which is at an angle with the line of sight. Although P-Cygni profiles in CVs are usually observed in the UV resonance lines, they can be also seen in the optical (Kafka & Honeycutt 2004, and references therein). Interestingly, this absorption S-wave is bluest at  $\varphi_a \simeq 0.5$ , just like the high-velocity emission S-wave characteristic of the SW Sex stars. A similar behaviour has been observed in the nova-like V592 Cas (Witherick et al. 2003), where the radial velocity curve of the absorption is also delayed with respect to that of the emission by 0.3 cycle.

### 5.1.2 Doppler tomography

In order to map the  $H\alpha$  line emission sites in velocity space we constructed a Doppler tomogram from the phase-folded data using the maximum entropy technique introduced by Marsh & Horne (1988) (Fig. 4). The Doppler image does not show either a ring-like structure typical of line emission originated in an accretion disc or any feature in the path of the gas stream. Instead, the bulk of emission is distributed on an elongated spot spread over the lower left quadrant

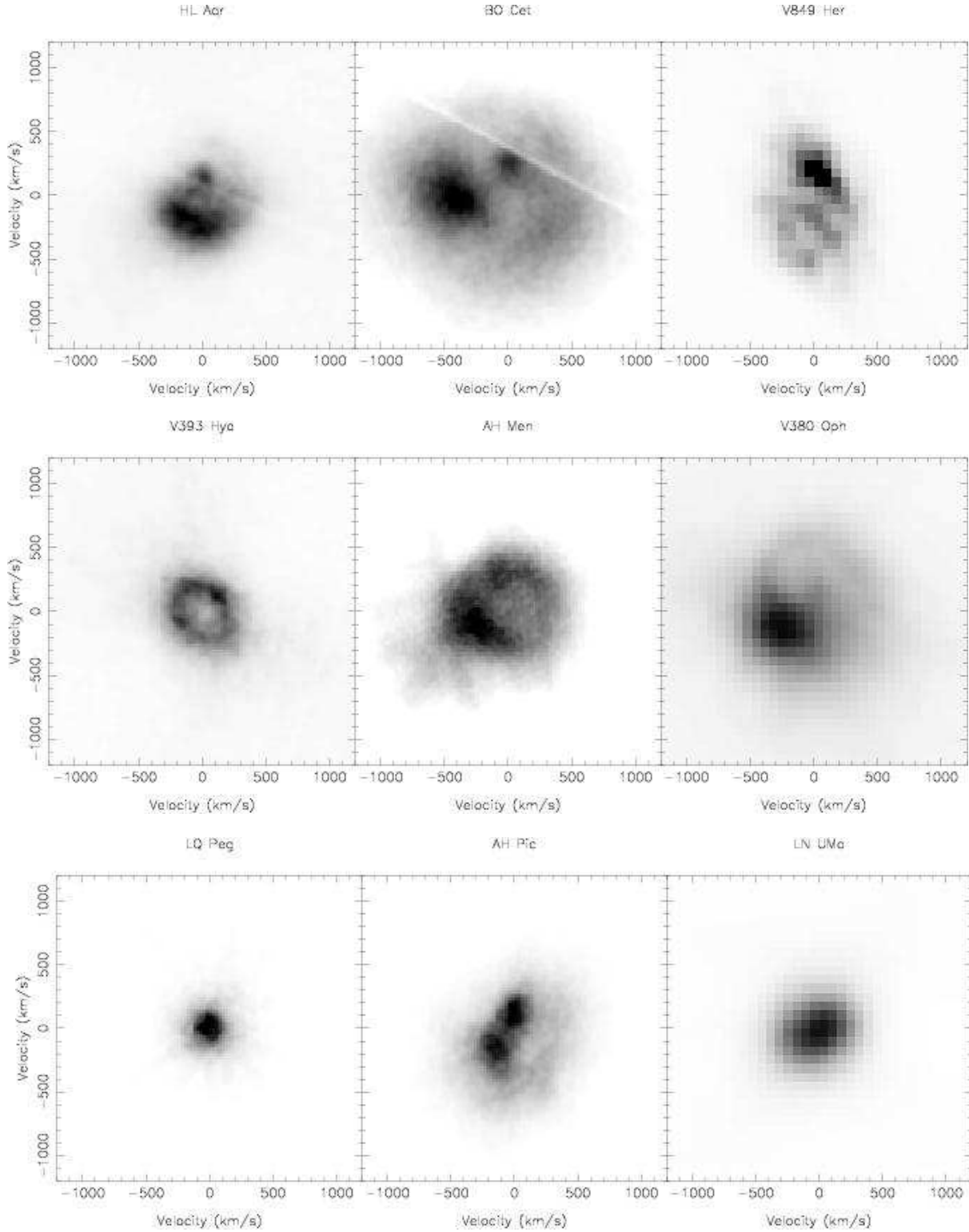


**Figure 4.** H $\alpha$  Doppler tomograms. No map has been computed for V992 Sco as the H $\alpha$  emission is still dominated by the nova shell.

at  $(V_x \sim -100, V_y \sim -200)$  km s $^{-1}$ , which is produced by the dominant broad S-wave observed in the trailed spectrogram. This is a common feature in the Doppler tomograms of the SW Sex stars. On the other hand, the narrow S-wave translates into a well-defined spot at  $(V_x \sim 0, V_y \sim +150)$

km s $^{-1}$  in the tomogram, where emission from the (likely irradiated) donor star would be placed.

### 5.1.3 Orbital inclination

The detection of an absorption S-wave in H $\alpha$  with maximum blue velocity at  $\varphi_a \sim 0.5$ —which may originate in a mass outflow—makes it very interesting to explore whether or not HL Aqr is viewed at a similar inclination as the emission-line dominated, non-eclipsing SW Sex stars ( $i \sim 60^\circ - 70^\circ$ ). In order to do so, estimates of the stellar masses have to be assumed. We will estimate the mass of the secondary star,  $M_2$ , by interpolating in the  $M_2 - P_{\text{orb}}$  sequence of donor stars in CVs of Knigge (2006), and will assume a representative white dwarf mass of  $M_1 = 0.75 M_\odot$  (Patterson et al. 2005; Knigge 2006). Spline interpolation of Knigge’s mass sequence yields  $M_2 = 0.21 M_\odot$  for the orbital period of HL Aqr. A mass ratio of  $q = M_2/M_1 = 0.28$  is therefore obtained. From Kepler’s Third Law we get:

$$\frac{P_{\text{orb}} K_2^3}{2\pi G} = M_1 \left[ \frac{1}{q(1+q)} \right] \sin^3 i. \quad (1)$$

In order to resolve for the orbital inclination we need an estimate of  $K_2$ . As mentioned earlier, the narrow H $\alpha$  emission seen in the trailed spectrum is very likely produced in the irradiated inner hemisphere of the donor star. Thus, its radial velocity amplitude,  $K_{\text{irr}}$ , is actually a lower limit to  $K_2$  as the irradiation light-centre is displaced from the donor’s centre of mass towards the inner Lagrangian point ( $L_1$ ). The “ $K$ -correction” that has to be applied to  $K_{\text{irr}}$  depends on the mass ratio and on a factor ( $0 < f < 1$ ), which represents the distance from the donor star’s centre of mass to the light-centre of the irradiated region (Muñoz-Darias et al. 2005, and references therein) in the form:

$$K_2 = \frac{K_{\text{irr}}}{1 - f(1+q)}. \quad (2)$$

Two extreme cases are: (i) emission from  $L_1$  only, in which case  $f$  is just the distance from  $L_1$  to the donor star’s centre of mass in units of the binary separation,  $R_{L_2}/a$ ; and (ii) emission from the limb of the irradiated hemisphere of the donor star. In the second case, and assuming a spherical Roche lobe when far from  $L_1$ ,  $f \simeq (R_{L_2}/a)^2$ . The former case is merely theoretical, and a more realistic upper limit to  $f$  can be obtained by modelling of the emission lines formed on the heated face of the secondary star (see equation for  $f(\alpha = 0^\circ)$  in Muñoz-Darias et al. 2005).

For HL Aqr, a sine fit to the radial velocities of the donor emission yields  $K_{\text{irr}} \simeq 159 \text{ km s}^{-1}$ . On the other hand, we get  $f(\alpha = 0^\circ) \simeq 0.27$ , and  $f \simeq 0.08$  for maximum irradiation (using the  $R_{L_2}/a$  equation given by Eggleton 1983). We therefore obtain (Eq. 2)  $177 < K_2 < 244 \text{ km s}^{-1}$ , so the orbital inclination of HL Aqr must lie in the range  $19^\circ < i < 27^\circ$ , much lower than in the emission-dominated, non-eclipsing SW Sex stars. Note that  $M_1$  and  $M_2$  (and therefore  $q$ ) have been assumed. If our mass estimates were close to the actual values, the fact that we see an *absorption* S-wave with maximum blueshift at  $\varphi_a \simeq 0.5$  might be a direct consequence of the much lower inclination of HL Aqr, which seems to support the hypothesis of a mass outflow with significant vertical motion in the system.

### 5.1.4 SW Sex class membership

HL Aqr is definitely not a “typical” SW Sex star. Whilst it exhibits single-peaked emission lines, the radial velocity curve of the H $\alpha$  line wings does not show a phase delay with respect to the motion of the white dwarf. Instead, the He I  $\lambda 6678$  emission line crosses from red to blue  $\sim 0.1$  orbital cycle *earlier* than expected. Moreover, a S-wave with maximum blue excursion at  $\varphi_a \simeq 0.5$  and blueshifted by  $\sim 1000 \text{ km s}^{-1}$ , is observed. Remarkably, this component is seen in absorption, not in emission as is commonly observed in the SW Sex stars. However, the similar phasing and the much lower orbital inclination of HL Aqr may point to an interesting connection. In this regard, it is possible that the high-velocity component originates in a mass outflow. Line emission from the wind dominates at higher inclinations, whilst P-Cygni absorption is the rule in nearly face-on systems (see e.g. Drew 1997). In addition, the prototypical phase-0.5 absorption is absent. This is not unexpected, as the narrow emission lines already sit on significant absorption. It is therefore plausible that the transient absorption can be only seen as transient in the high inclination SW Sex stars. Finally, the Doppler tomogram shows the bulk of emission distributed over its lower left quadrant, a typical signature of the SW Sex stars. In summary, HL Aqr shows features that point to a SW Sex nature. The differences with the canonical ones might be due to its much lower inclination.

## 5.2 BO Cet

BO Cet (= Cet 4, 1H 0204–023, PB 6656) is listed as a nova-like CV in Downes et al. (2005). The optical spectrum obtained by Zwitter & Munari (1995) shows a blue continuum with broad, single-peaked emission lines of H I and weaker, double-peaked He I. The presence of a strong He II  $\lambda 4686$  emission line reveals a source of ionising photons within the binary, as observed in magnetic CVs and SW Sex stars. However, there is no orbital phase-resolved spectroscopic analysis in the literature even though BO Cet is a fairly bright CV ( $V \sim 14 - 15$ ). Downes et al. (2005) quote an orbital period of 0.1398 d (= 3.36 h) obtained from intensive photometric coverage compiled at the Center for Backyard Astrophysics<sup>3</sup>.

### 5.2.1 H $\alpha$ radial velocities and trailed spectrum

Our spectra show a relatively broad (FWHM  $\simeq 1300 \text{ km s}^{-1}$ ) H $\alpha$  emission line, indicative of an intermediate-high orbital inclination, with a half-width at zero-intensity (HWZI) reaching  $\sim 4000 \text{ km s}^{-1}$ . Alas, our data only cover one orbital cycle, which is insufficient for an accurate orbital period determination. In spite of that, we measured the radial velocity variation of the H $\alpha$  emission line by two methods: cross-correlation of the individual profiles with (i) a single FWHM =  $300 \text{ km s}^{-1}$  Gaussian template, and (ii) two FWHM =  $200 \text{ km s}^{-1}$  Gaussians separated by  $3500 \text{ km s}^{-1}$  (the double Gaussian technique of Schneider & Young 1980). A sine fit to the core velocities

<sup>3</sup> The news note on the orbital period of BO Cet can be found at <http://cba.phys.columbia.edu/communications/news/2002/october29-a.html>



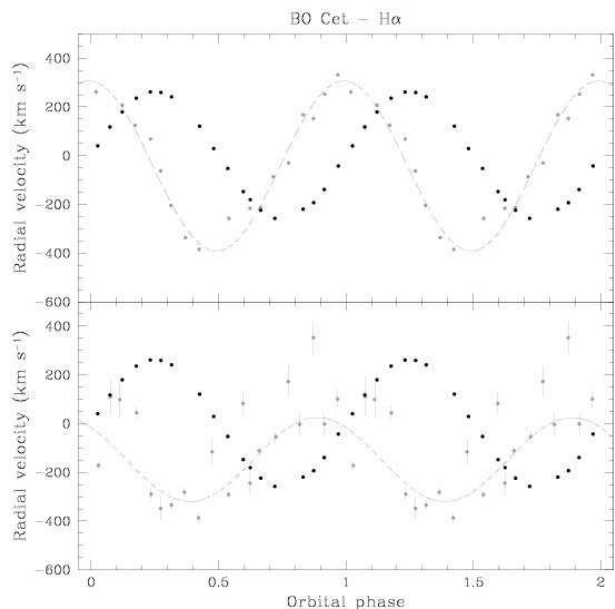


**Figure 5.** *Top:* phase folded ( $P_{\text{orb}} = 0.1398$  d)  $\text{H}\alpha$  radial velocity curve of BO Cet obtained by cross-correlation with a single Gaussian template of  $\text{FWHM} = 300$   $\text{km s}^{-1}$  (gray) and the best sine fit (dashed line); and radial velocity curve of the  $\text{H}\alpha$  emission from the donor star (black). There is a 0.24-cycle shift between the two. *Bottom:* same but applying the double-Gaussian technique with  $\text{FWHM} = 200$   $\text{km s}^{-1}$  and a Gaussian separation of  $3500$   $\text{km s}^{-1}$  (gray). The  $\text{H}\alpha$  wings are also delayed by 0.14-cycle with respect of the motion of the white dwarf. All the curves have been averaged into 20 phase bins. Some clearly deviant points have been removed for clarity. The orbital cycle has been plotted twice.

yields a period of  $\simeq 0.14$  d. This is consistent with the photometric value mentioned earlier, which we adopt as the orbital period.

An initial  $\text{H}\alpha$  trailed spectrum revealed a narrow emission S-wave with an amplitude of  $\sim 200 - 300$   $\text{km s}^{-1}$  and a likely origin on the heated face of the secondary star. In order to obtain absolute phases we proceeded in the same way as with HL Aqr (Sect. 5.1.1), obtaining  $T_0(\text{HJD}) = 2453640.7633 \pm 0.0001$  and  $K_{\text{irr}} = 262 \pm 2$   $\text{km s}^{-1}$ . The phase folded  $\text{H}\alpha$  radial velocity curves are presented in Fig. 5. The line core lags the motion of the white dwarf by 0.24 cycle. In addition, the wings are also delayed by 0.14 cycle and are significantly blueshifted, which clearly depicts the risk of adopting the amplitude of the wings radial velocity curve as the true radial velocity of the white dwarf ( $K_1$ ) for mass measurements (a common practice as seen in the literature).

The  $\text{H}\alpha$  trailed spectrum of BO Cet (Fig. 3) displays several interesting features. The line profile is dominated by an emission S-wave with an amplitude of  $\sim 300$   $\text{km s}^{-1}$  and bluest velocity at  $\varphi_a \simeq 0.5$ . This component shows maximum intensity in the  $0.65 - 0.95$  phase interval, and probably a secondary maximum at  $\varphi_a \sim 0.3$ . Intensity minima take place at  $\varphi_a \simeq 0.5$  and  $\varphi_a \simeq 0$ , when the EW of the line core is minimum. Moreover, the line wings are shaped by a high-velocity S-wave clearly visible up to  $-2000$   $\text{km s}^{-1}$ . This component is clearly pulsed, which is confirmed by a non-phase folded trailed spectra (not shown).

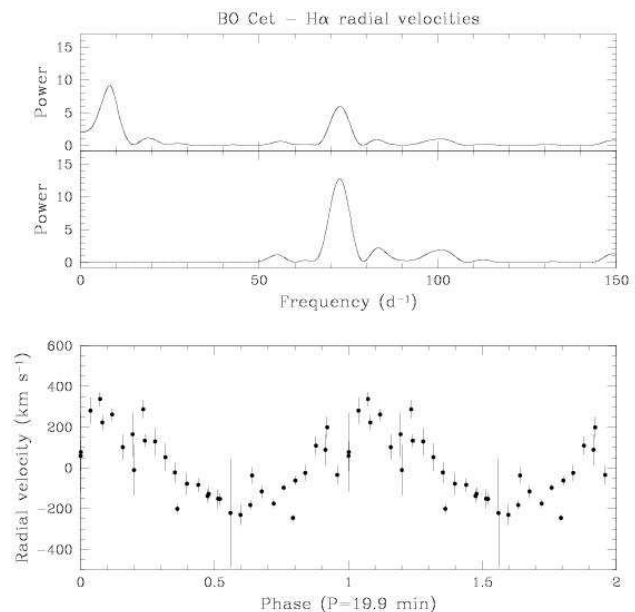


**Figure 6.** *Top panel:* Scargle periodogram computed from the radial velocity curve of the  $\text{H}\alpha$  wings in BO Cet. Strong peaks centered at both the orbital frequency and at  $\nu = 72.5$   $\text{d}^{-1}$  are apparent. *Middle panel:* Scargle periodogram after pre-whitening the data at the orbital period. The data were detrended by subtracting a boxcar-smoothed version of the curve in order to remove the long time-scale variations. *Bottom panel:* detrended  $\text{H}\alpha$  velocities folded on the 19.9-min period. A full cycle has been repeated for clarity.

### 5.2.2 Emission-line flaring

Emission-line rapid variability is often observed in intermediate polars (e.g. FO Aqr Marsh & Duck 1996) and SW Sex stars (e.g. BT Mon, Smith, Dhillon & Marsh 1998; LS Peg, Rodríguez-Gil et al. 2001; V533 Her, Rodríguez-Gil & Martínez-Pais 2002; DW UMa, V. Dhillon, private communication; and RX J1643.7+3402, Martínez-Pais, de la Cruz Rodríguez & Rodríguez-Gil 2007).

This fast oscillation is responsible for the scatter observed in the radial velocity curve of the  $\text{H}\alpha$  wings (Fig. 5, bottom panel). In fact, the non-phase folded wing velocities clearly exhibit a short time-scale oscillation at  $\sim 15 - 20$  min. In order to search for periodicities we computed the Scargle periodogram shown in Fig. 6 (top panel), which contains two strong peaks: one at the orbital frequency and another one at  $\nu \simeq 72.5$   $\text{d}^{-1}$ . After subtracting the orbital modulation, another periodogram was calculated, showing the main peak at a period of  $19.9 \pm 0.9$  min (the quoted uncertainty is half the FWHM of the peak). Although the peaks are significant, we can only state that this oscillation is coherent for at least 10 cycles. Therefore, a much longer spectroscopic coverage is needed in order to confirm whether this radial velocity variation is produced by a stable clock in the system. In such a case, the 19.9-min period should be related to the spin period of a magnetic white dwarf as it happens in intermediate polars like V1025 Cen (Buckley et al. 1998), DW Cnc (Rodríguez-Gil et al. 2004), and HS 0943+1404 (Rodríguez-Gil et al. 2005).

With the aim of searching for rapid variations, we also

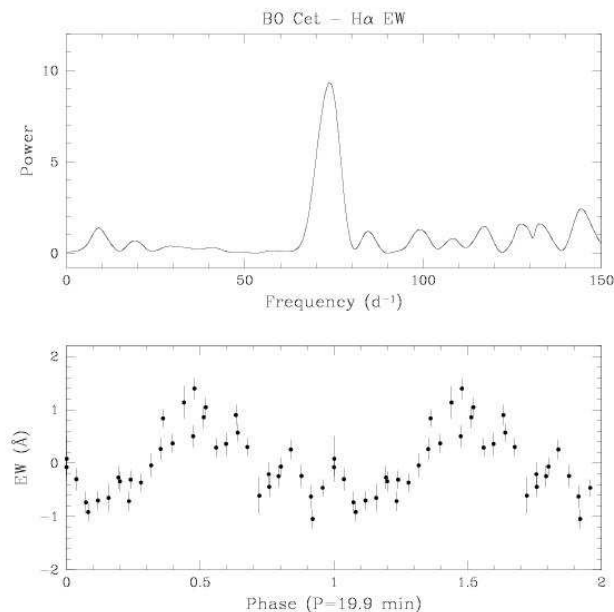


**Figure 7.** *Top panel:* Scargle periodogram computed from the EW curve of the  $H\alpha$  blue wing of BO Cet pre-whitened at the orbital frequency. *Bottom panel:* detrended  $H\alpha$  EWs folded on the 19.9-min period. A full cycle has been repeated for clarity.

measured the EW curve of the  $H\alpha$  line blue wing (the high-velocity emission S-wave is best seen in the blue) in the velocity interval  $(-3500, -1200)$   $\text{km s}^{-1}$ . After prewhitening at the orbital frequency, a Scargle periodogram was computed (Fig. 7). A strong peak centred at  $19.6 \pm 0.9$  min, consistent with the observed periodicity in the radial velocity curves, is apparent.

### 5.2.3 Doppler tomography

The  $H\alpha$  Doppler tomogram of BO Cet is presented in Fig. 4, where two  $H\alpha$  emission sites are clearly observed. A small, concentrated emission spot is located at  $(V_x \sim 0, V_y \sim +260)$   $\text{km s}^{-1}$ , just where emission from the donor star is expected to lie. In fact, the  $V_y$  position of the spot on the map coincides with the amplitude of the radial velocity curve of the donor emission ( $K_{\text{irr}} = 262$   $\text{km s}^{-1}$ ). In addition, a broad spot is seen in the lower left quadrant of the Doppler map, approximately centred on  $(V_x \sim -400, V_y \sim -10)$   $\text{km s}^{-1}$ . This is a characteristic feature of the tomograms of the SW Sex stars.

### 5.2.4 Orbital inclination

Adopting the component masses  $M_1 = 0.75 M_\odot$  and  $M_2 = 0.22 M_\odot$  for BO Cet (see Sect. 5.1.3), we obtain a mass ratio of  $q = 0.29$ . The extreme limits to the  $K$ -correction provide a radial velocity amplitude for the companion star in the range  $292 < K_2 < 407$   $\text{km s}^{-1}$ , which implies an orbital inclination in the interval  $35^\circ < i < 52^\circ$ .

### 5.2.5 SW Sex class membership

The above analysis qualifies BO Cet as a new non-eclipsing SW Sex star. The emission lines are mainly single peaked, with the exception at phase 0.5, when they turn double peaked. Phase 0.5 is also the instant of minimum EW of the line core. In addition,  $H\alpha$  exhibits a clear emission S-wave with maximum blue velocity at phase 0.5, which translates into an elongated emission spot in the lower left quadrant of the Doppler tomogram. Also, both the core and wings radial velocity curves are delayed with respect of the motion of the white dwarf. Finally, BO Cet displays emission-line flaring with a periodicity of 19.9 min.

A word of caution should be raised regarding the actual orbital period of BO Cet. In our study we have adopted a photometric period which can not be *a priori* discarded as, for example, a superhump period. Although the fact that Patterson’s analysis yielded a single periodicity supports a pure orbital origin, we should bear in mind that many SW Sex stars show positive and/or negative permanent superhumps (see e.g. Patterson 1995; Patterson et al. 2002; Stanishev et al. 2002; Patterson et al. 2005). Hence, only a more extensive spectroscopic coverage will provide the actual orbital period.

## 5.3 V849 Her

V849 Her (= PG 1633+115) was tentatively identified as a 15-mag CV in the Palomar-Green survey (Green, Schmidt & Liebert 1986). Its optical spectrum displays weak  $H\alpha$  emission and  $H\beta$  absorption with a continuum showing variations with a time-scale of days (Ringwald 1993). Extensive  $V$ -band photometry performed by Misselt & Shafer (1995) revealed a 0.5-mag drop in brightness and a modulation at a period of  $\sim 3.5$  h. Alas, the analysis of the light curves did not provide an accurate orbital period. A further optical spectrum obtained by Munari & Zwitter (1998) confirmed the presence of a very weak  $H\alpha$  emission line superposed on a broader absorption. An even weaker  $H\beta$  emission can be seen at the bottom of a dominating  $H\beta$  absorption trough.

Our WHT flux-calibrated, average spectrum is presented in Fig. 8. Broad absorption lines dominate blueward of  $H\beta$ , whereas the  $H\alpha$  line is mostly in emission and shows a single-peaked profile. A weak  $\text{He II } \lambda 4686$  emission line is also observed. On the basis of the observed long-term brightness changes it has been argued (Ringwald 1993) that V849 Her might be a dwarf nova. Our average spectrum, however, is very similar to Munari & Zwitter’s, suggesting that either the system comes into outburst quite frequently or it shows on most occasions an absorption-dominated spectrum. Thus, V849 Her is most likely a low-inclination nova-like, or possibly a Z Cam dwarf nova. Long term monitoring of its visual brightness is necessary to differentiate between the two possibilities.

### 5.3.1 $H\alpha$ radial velocities and trailed spectrum

With the aim of obtaining the orbital period of V849 Her we measured the radial velocities of the  $H\alpha$  emission line. The best results were obtained using the double-Gaussian technique with  $\text{FWHM} = 200$   $\text{km s}^{-1}$  and a Gaussian separation of  $900$   $\text{km s}^{-1}$ . A sine fit to the velocities provided a period

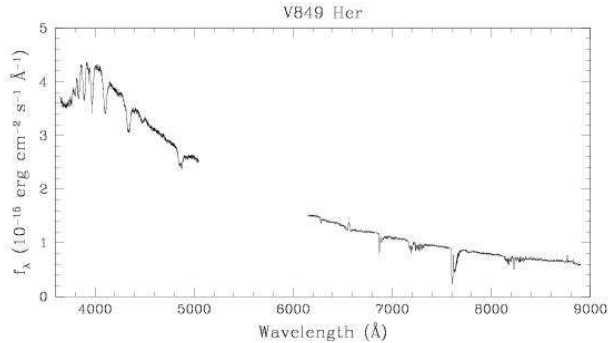


**Figure 8.** WHT flux-calibrated, average spectrum of V849 Her. No telluric absorption correction has been applied.

of  $3.15 \pm 0.48$  h, but the short interval our spectroscopic data covers (only 2.64 h) prohibits us from reaching any firm conclusion regarding the actual orbital period. Even though the orbital period of V849 Her is not a settled issue, we folded the spectroscopic data on the period given by the sine fit to the velocities and averaged the spectra into 20 orbital phase bins.

A preliminary H $\alpha$  trailed spectrogram computed from the phase-folded data (using the  $T_0$  from the fit to the velocities) shows an emission S-wave extending up to  $\pm 500$  km s $^{-1}$  and reaching its bluest velocity at  $\varphi_r \sim 0.3 - 0.4$ . There is also another emission component moving with smaller velocity amplitude ( $\sim 200$  km s $^{-1}$ ) which has maximum intensity at  $\varphi_r \sim 0.4 - 0.5$ . The phase-binned spectra show alternating double-peaked and single-peaked H $\alpha$  profiles, which supports the presence of at least two emission components. The emission component with smaller velocity may originate on the heated inner face of the secondary star. Its maximum strength at  $\varphi_r \sim 0.5$  seems to support this origin. This will allow us to measure an absolute ephemeris so that the higher velocity component can be appropriately phased. In order to do so we applied the same technique we used with HL Aqr and BO Cet, obtaining  $T_0(\text{HJD}) = 2453513.536 \pm 0.005$  and  $K_{\text{irr}} = 257 \pm 18$  km s $^{-1}$ . The phase-binned H $\alpha$  radial velocity curves are presented in Fig. 9. There is no phase delay between the radial velocities measured with the double-Gaussian technique and the white dwarf motion which, on the other hand, is true only if the assumption of emission from the donor star is correct. Alas, the signal-to-noise ratio of our data is not adequate to check whether the He I  $\lambda 6678$  emission line is phase-shifted or not.

### 5.3.2 Doppler tomography

The H $\alpha$  Doppler map of V849 Her is shown in Fig. 4. Its main feature is an emission spot located at the position of the donor star ( $V_x \sim 0, V_y \sim +250$ ). The other elongated emissions are likely artifacts due to the poor phase sampling. The characteristic SW Sex emission at the lower left quadrant is not observed.

### 5.3.3 Orbital inclination

In this case, following our usual analysis,  $M_1 = 0.75 M_\odot$  and  $M_2 = 0.20 M_\odot$ , which results in a mass ratio of  $q = 0.27$ .

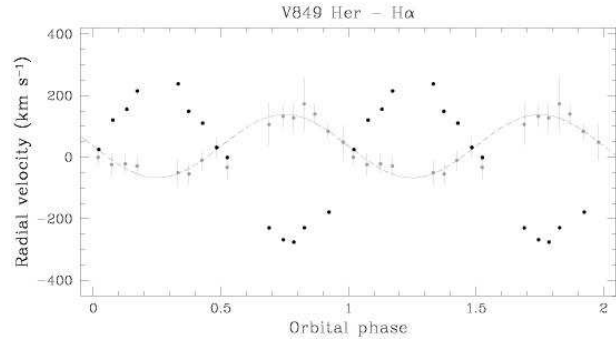


**Figure 9.** H $\alpha$  radial velocity curve of V849 Her obtained by using a double-Gaussian template of FWHM = 200 km s $^{-1}$  and a Gaussian separation of 900 km s $^{-1}$  (gray) and the best sine fit (dashed line); and radial velocity curve of the H $\alpha$  emission from the donor star (black). There is no phase delay between the two. A full orbital cycle has been repeated for clarity.

The radial velocity amplitude of the secondary star should therefore lie in the interval  $296 < K_2 < 389$  km s $^{-1}$ , which translates into an orbital inclination range of  $33^\circ < i < 45^\circ$ . These numbers are very similar to the results obtained for BO Cet but, clearly, both systems behave differently. If we assume a plausible  $K$ -correction of  $K_{\text{irr}}/K_2 \simeq 0.7$  (see Figure 4 in Muñoz-Darias et al. 2005), we obtain  $K_2 \simeq 367$  km s $^{-1}$ . Identifying the amplitude of the radial velocity curve of the disc emission with  $K_1$ , we get  $q = K_1/K_2 \simeq 0.27$ , which matches the assumed value. In the SW Sex stars, the presence of the high-velocity emission S-wave tends to increase the amplitude of the wing velocities which, together with the characteristic phase shifts, suggests that the bulk of emission is not coming from an axisymmetric structure around the white dwarf. This does not seem the case in V849 Her.

### 5.3.4 SW Sex class membership

The spectroscopic behaviour of V849 Her does not seem to qualify it as a SW Sex star. Nevertheless, better quality spectra with better sampling would be desirable to validate or disprove its SW Sex nature.

As a final note, the optical spectrum of V849 Her is very similar to that of a number of nova-likes found in the Hamburg Quasar Survey (e.g. HS 0139+0559, HS 0229+8016, and HS 0642+5049, Aungwerojwit et al. 2005), which are dominated by absorption and also have orbital periods in the range 3 – 4 h. Because of their inconspicuous spectroscopic, photometric, and X-ray properties, this type of system may be quite frequent, with a significant number of objects still to be identified. Together with V849 Her, these systems are likely viewed at intermediate-low inclinations, so we are therefore looking directly at optically thick disc material. Hence, broad line absorption may dominate the spectra of nearly face-on systems. Such dominance is actually seen in the UX UMa nova-likes.

## 5.4 V393 Hya

V393 Hya (= EC 10578–2935) was listed as a CV and tentatively classified as a nova-like by Kilkenny et al. (1997), an identification later supported by the weak Balmer

lines observed by Sefako et al. (1999) in its optical spectrum. The system shows a variable emission pattern in which a spectrum with weak Balmer, He II  $\lambda 4686$ , and Bowen blend emissions (Chen et al. 2001) can switch to a flat and featureless continuum with only H $\alpha$  in emission (Dall & Schmidtobreick 2004). The weakness of the emission lines suggests a rather hot accretion disc and, therefore, is indicative of the high mass transfer rate characteristic of nova-like CVs. In addition, the emission lines are very narrow, showing a H $\alpha$  full width at zero intensity (FWZI) of only  $\sim 700 - 900 \text{ km s}^{-1}$ , which indicates a low orbital inclination. In fact, Chen et al. were not able to extract any useful radial velocity information from the line profiles.

Like BO Cet, V393 Hya was also subject to extensive photometric scrutiny by the observers associated to the Center for Backyard Astrophysics, who found a periodicity of 0.1346 d (= 3.23 h) in the phase-resolved light curves<sup>4</sup>.

#### 5.4.1 H $\alpha$ radial velocities, trailed spectrum, and Doppler tomogram

The NTT average spectrum shown in Fig. 1 exhibits double-peaked H $\alpha$  emission together with a flat-topped He I  $\lambda 6678$  line. Contrary to previous works, we measured FWZI  $\gtrsim 2000 \text{ km s}^{-1}$ , a factor of two higher than reported by other authors. The radial velocity curve of the H $\alpha$  line was computed by cross-correlation of the individual profiles with a double-Gaussian template with FWHM =  $200 \text{ km s}^{-1}$  and a Gaussian separation of  $800 \text{ km s}^{-1}$ . A Scargle periodogram of the H $\alpha$  velocities (not shown) suggests an orbital period of 0.14 – 0.15 d, consistent with the photometric periodicity. However, our limited coverage (0.9 h and 2.6 h on April 17 and 18, respectively) is clearly insufficient to provide an accurate orbital period, so we use the photometric estimate.

The H $\alpha$  trailed spectra of V393 Hya (Fig. 3; relative orbital phases) only shows the orbital motion of the double-peaked profile and enhanced wings reaching  $\sim \pm 500 \text{ km s}^{-1}$ . A much better spectral resolution and signal-to-noise ratio are needed to resolve any component moving beneath the two peaks. The Doppler map (Fig. 4) solely reveals a ring of emission, which is the result of the double-peaked shape of the H $\alpha$  emission line. In spite the poor quality of our data, V393 Hya does not seem to behave as a SW Sex star.

## 5.5 AH Men

The bright ( $V \simeq 13$ ) counterpart of the X-ray source 1H 0551–819 has at first been regarded as an intermediate polar cataclysmic variable (Warner & Wickramasinghe 1991; Wu & Wickramasinghe 1991), even before being identified as a nova-like CV by Buckley et al. (1993). These authors obtained 79 h of photometric data which revealed a periodicity of 3.34 h. Apart from erratic flickering the light curves also showed quasi-periodic oscillations (QPOs) with preferred time-scales in the range  $\sim 600 - 2500 \text{ s}$ . The light curve of AH Men also displayed dips at maximum light which were suggested to be shallow eclipses, but this point was

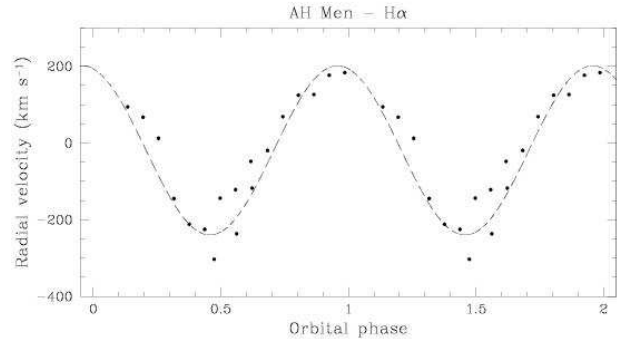


**Figure 10.** H $\alpha$  radial velocity curve of AH Men. A 0.2-cycle delay with respect to the expected red-to-blue crossing is seen (see text for details on the assumed ephemeris). The dashed curve is the best sine fit to the data. A full cycle has been repeated.

never confirmed. In such a case the orbital inclination of the CV would be around  $70^\circ$ .

Patterson (1995) secured 190 h of high-speed photometry of AH Men finding a stable period of 2.95 h which is therefore believed to be the orbital period of the system. Lower coherence signals at 3.05 h and 2.88 h were also found, suggesting the presence of positive (apsidal) and negative (nodal) superhumps, respectively. This is supported by the detection of two much longer periodicities close to 4 d likely associated with the corresponding precession periods of an eccentric, wobbling accretion disc. On the other hand, the high frequency range is characterised by oscillations at  $\sim 1020 - 1320 \text{ s}$  with a probable white dwarf spin period of either 1040 s or 2080 s.

The average optical spectrum of AH Men reported by Buckley et al. (1993) exhibited double-peaked Balmer and He I emission lines and a single-peaked He II  $\lambda 4686$  emission, the latter indicating a moderate level of excitation of the accretion flow. Buckley et al. performed a radial velocity study from spectroscopic data spanning 5 h obtaining a periodicity of  $3.1 \pm 0.3 \text{ h}$  and a  $K$ -amplitude of  $\sim 140 \text{ km s}^{-1}$ . This period is consistent with Patterson’s findings but the spectroscopic data alone were not sufficient to unambiguously confirm the orbital period of AH Men.

The UV spectrum presented by Mouchet et al. (1996) is similar to that of the non-eclipsing SW Sex star V795 Her (Prinja, Drew & Rosen 1992). Both exhibit transient absorptions in the C IV  $\lambda 1549$  line proposed to be due to an accretion disc wind but, unlike V795 Her, the UV spectrum of AH Men shows the C IV  $\lambda 1549$  line predominantly in emission, suggesting a higher inclination (V795 Her is seen at  $\sim 53^\circ - 56^\circ$ , Casares et al. 1996; Rodríguez-Gil et al. 2001). Gänsicke & Koester (1999) derived a lower limit to the distance of  $d = 150 \text{ pc}$  from the non-detection of the donor star, and showed that the UV spectrum of AH Men can be qualitatively modelled with an optically thick accretion disc model at a distance of  $\sim 200 \text{ pc}$ .

#### 5.5.1 H $\alpha$ radial velocities and trailed spectrum

The average H $\alpha$  profile (Fig. 1) has FWHM  $\simeq 940 \text{ km s}^{-1}$  and displays asymmetric wings disappearing into the continuum at velocities of  $\sim \pm 4000 \text{ km s}^{-1}$ .

<sup>4</sup> CBA news note on V393 Hya at: <http://cba.phys.columbia.edu/communications/news/2003/april27.html>

We measured the radial velocity curve of the H $\alpha$  emission line by cross correlation of the individual profiles with a double Gaussian template (1600 km s<sup>-1</sup> separation, FWHM = 200 km s<sup>-1</sup>). Adopting the orbital period reported by Patterson (1995),  $P_{\text{orb}} = 0.122992$  d, a sine fit to the radial velocity curve yields a time of red-to-blue crossing of  $2453477.5667 \pm 0.0002$  (HJD). The subsequently phase-folded trailed spectrum showed a high-velocity emission S-wave with maximum blueshift at  $\varphi_r \sim 0.3$ . Note that in the eclipsing SW Sex stars (for which accurate eclipse ephemeris are available) this happens at  $\varphi_a \sim 0.5$  (see Sect. 3). Hence, the actual time of inferior conjunction of the donor star in AH Men should take place  $\sim 0.2$  orbital cycle earlier than the  $T_0$  provided by the radial velocity curve, that is,  $T_0 = 2453477.5421 \pm 0.0002$  (HJD).

The trailed spectrum (Fig. 3) clearly shows a high-velocity S-wave with an amplitude of  $\sim 1000$  km s<sup>-1</sup> and a central absorption when the S-wave is at its bluest excursion, a hallmark of the SW Sex stars. In fact, the EW of the line has a minimum at  $\varphi_a \simeq 0.5$ . It does not appear to show flaring, as can be also seen in the trailed spectrum. Contrary to HL Aqr and BO Cet, no narrow emission from the donor star is apparent.

### 5.5.2 Doppler tomography

The H $\alpha$  Doppler map of AH Men (Fig. 4) shows the characteristic emission pattern of the SW Sex stars, with emission concentrated in the lower left quadrant of the tomogram. There might be also an emission spot close to the expected location of the secondary star at ( $V_x \sim -80, V_y \sim +290$ ) km s<sup>-1</sup>. However, the trailed spectrum does not show an apparent emission with the phasing of the donor star.

### 5.5.3 SW Sex class membership

The H $\alpha$  emission of AH Men is characterised by a high-velocity S-wave which maximum blue velocity at  $\varphi_a \sim 0.5$ . The single-peaked line profiles reach minimum EW at the same phase, which is probably due to a crossing absorption component. Additionally, the radial velocity curve of the line wings shows a phase delay of  $\sim 0.2$  orbital cycle with respect to the white dwarf motion. Furthermore, the H $\alpha$  Doppler tomogram displays the characteristic emission in its lower-left quadrant. All of this represent defining features of the SW Sex class. Hence, we classify AH Men as a SW Sex star. Finally, it would be desirable to perform phase-resolved spectroscopy with better time resolution to check whether the rapid oscillation in the light curve has a counterpart in the emission lines.

## 5.6 V380 Oph

The first spectroscopic analysis of V380 Oph showed the system to have strong Balmer emission lines on top of a blue continuum (Shafter 1985). Shafter concluded that the system is a high mass transfer nova-like CV. He also performed radial velocity studies and derived an orbital period of  $P_{\text{orb}} = 3.8$  h. Analysis of archival plates shows that the brightness of V380 Oph occasionally drops by  $\sim 2.5$  mag reaching a photographic magnitude of  $B_{\text{pg}} \simeq 17$

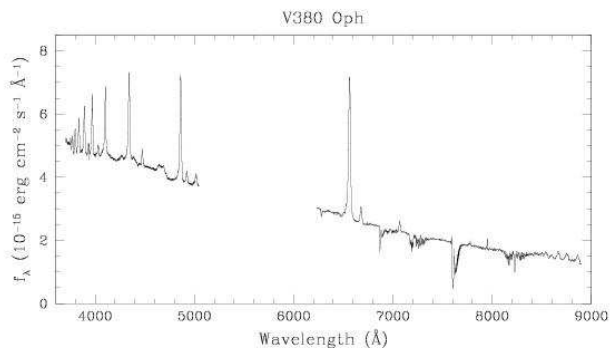


**Figure 11.** WHT flux-calibrated, average spectrum of V380 Oph. No telluric absorption correction has been applied.

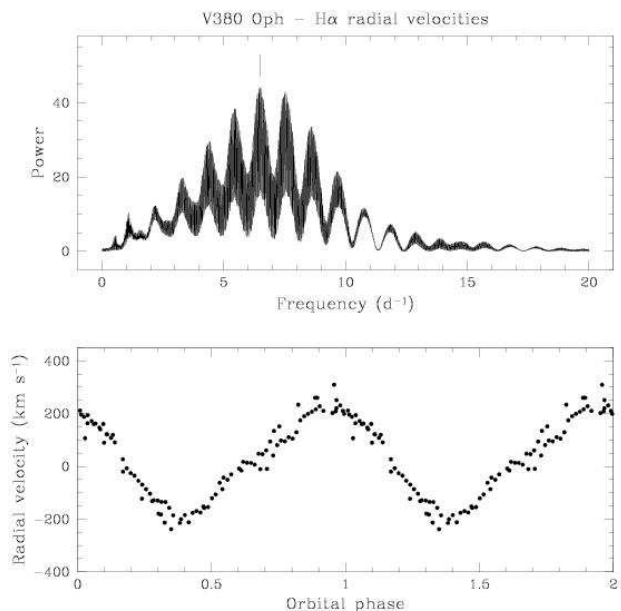


**Figure 12.** *Top:* Scargle periodogram of the H $\alpha$  radial velocity curves of V380 Oph. The adopted orbital period of 0.154107 d corresponds to the marked peak. *Bottom:* phase-folded H $\alpha$  radial velocity curve (no phase binning has been applied) showing a 0.15-cycle delay with respect to expected red-to-blue crossing time (see text for details on the assumed  $T_0$ ). A full cycle has been repeated.

(Shugarov et al. 2005). These low states seem to last for about one year and qualify V380 Oph as a VY Scl star. Shugarov et al. also found two periodicities in their optical light curves: 0.148 d and 4.5 d. The former is quite close to the spectroscopic period reported by Shafter whilst the latter may be related to disc precession.

The average WHT spectrum of V380 Oph is shown in Fig. 11. It is dominated by strong, single-peaked Balmer emission lines. Much weaker He I, He II  $\lambda 4686$ , and the Bowen blend are also seen. The average NTT H $\alpha$  profile (Fig. 1) has an EW of 41 Å (Table 2), about twice the value given by Shafter (1985). Photometry made on our NTT acquisition images confirmed that the brightness of V380 Oph was almost the same as during Shafter's observations.

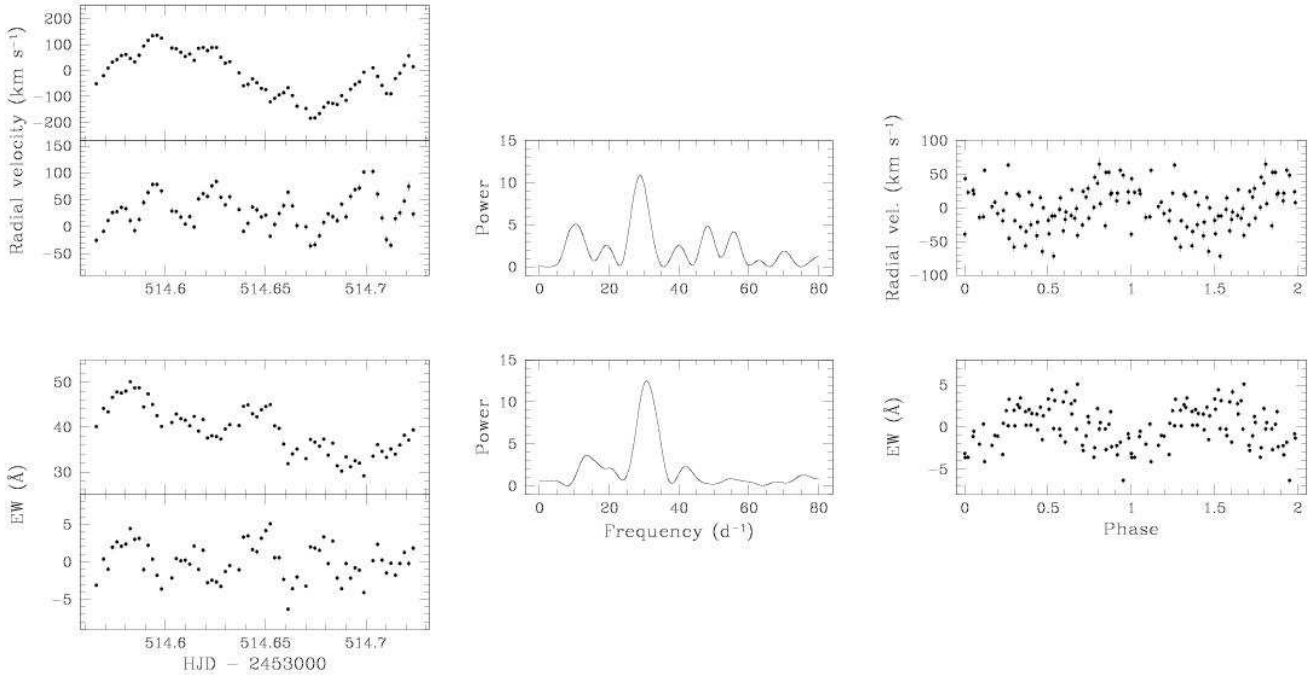


**Figure 13.** *Top left:* actual (*top*) and detrended (*bottom*)  $H\alpha$  radial velocity curves of V380 Oph. *Bottom left:* the same for the EWs. *Middle panel:* Scargle periodograms from the detrended  $H\alpha$  radial velocities (*top*) and EWs (*bottom*). *Right panel:* the detrended radial velocities (*top*) and EWs (*bottom*) folded on the 46.7-min period. The orbital cycle has been plotted twice.

### 5.6.1 $H\alpha$ radial velocities and trailed spectrum

The  $H\alpha$  radial velocity curves of V380 Oph were obtained by applying the double Gaussian technique to both the NTT and WHT individual profiles, adopting a Gaussian separation of  $400 \text{ km s}^{-1}$  and  $\text{FWHM} = 200 \text{ km s}^{-1}$ . The Scargle periodogram (Fig. 12) shows the highest peak centred at  $\nu \simeq 6.49 \text{ d}^{-1}$ , which corresponds to an orbital period of  $P = 0.154107 \pm 0.000001 \text{ d}$  ( $= 3.70 \text{ h}$ ), where the uncertainty comes from a sine fit to the velocities. Our period measurement supersedes the less accurate value of  $0.16 \text{ d}$  reported by Shafter (1985). The photometric period measured by Shugarov et al. (2005) is 3.8 per cent *shorter* than the orbital period, suggesting the occurrence of a negative (nodal) superhump. As in the case of AH Men, the detection of a much longer period at  $\sim 4 \text{ d}$  strongly supports the presence of an eccentric, wobbling accretion disc in V380 Oph.

A preliminary trailed spectrum (not shown) computed from the phase-binned data (using the  $T_0$  given by the above sine fit) shows a prominent, high-velocity S-wave with maximum blue velocity taking place at  $\varphi_r \sim 0.3$ . Once more, as this emission feature should be bluest at  $\varphi_a \sim 0.5$  in the SW Sex stars, a phase delay of  $\Delta\varphi \sim 0.2$  is suggested. After correcting for this offset we get a more realistic time of zero phase of  $T_0(\text{HJD}) = 2453514.61061 \pm 0.00008$ .

A new trailed spectrum is presented in Fig. 3. The line core is dominated by an emission S-wave with an amplitude of  $\sim 200 \text{ km s}^{-1}$ . In addition, there may be another similar amplitude, narrow S-wave which appears to reach maximum blue velocity at  $\varphi_a \sim 0.75$ . If our  $T_0$  is the correct one that emission component would be naturally placed on the donor star, presumably on its irradiated face. Unfortunately, it proved impossible to isolate this component in

order to confirm the ephemeris. Besides, an EW curve of the line core (between  $-300 \text{ km s}^{-1}$  and  $+300 \text{ km s}^{-1}$ ) reveals a minimum at  $\varphi_a \simeq 0.5$ , probably caused by the prototypical absorption that the SW Sex stars show at that orbital phase. On the other hand, a high-velocity S-wave reaching values as large as  $-3000 \text{ km s}^{-1}$  produces the line wings.

### 5.6.2 Emission-line flaring

The intensity of the high-velocity S-wave does not appear to be uniform, but follows a humpy pattern that is clearly visible in the blue wing, where the S-wave is best seen. This bears close similarity with what is seen in BO Cet and other SW Sex stars already mentioned in Sect. 5.2, and is likely caused by emission-line flaring. In order to probe for this possibility we computed a set of radial velocity curves of the  $H\alpha$  line for the longest data set (May 22), but this time choosing several Gaussian separations that entered the line wings. At a separation of  $1000 \text{ km s}^{-1}$  the radial velocity curve is still dominated by the orbital modulation but a variation at a much shorter time-scale ( $\sim 50 \text{ min}$ ) is also seen (Fig. 13). A similar oscillation is present in the EW curve of  $H\alpha$  obtained in the  $(-1200, 1200) \text{ km s}^{-1}$  velocity interval (Fig. 13).

With the aim of searching for periodicities we first detrended both the radial velocity and EW curves by subtracting a sine fit, and then computed Scargle periodograms. Both power spectra are dominated by a strong peak centred at  $\sim 31 \text{ d}^{-1}$ , which corresponds to a period of  $\sim 47 \text{ min}$ . A Gaussian fit to the peak in the EW periodogram gives  $46.7 \pm 0.1 \text{ min}$  (the error comes from a sine fit to the EW curve). At this point we have to rise a word of caution. The velocity and EW curves presented in Fig. 13 span slightly

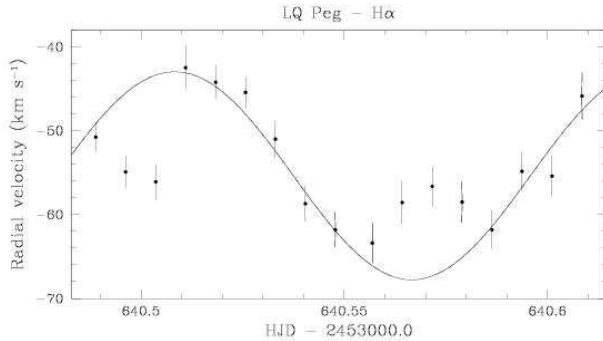


**Figure 14.**  $H\alpha$  radial velocity curve of LQ Peg. The solid line is the best sine fit to the data. The two points flanking 640.5 and three points about 640.52 have been excluded from the fit.

more than an orbital cycle, hence, they contain only five 47-min cycles. This alone is not clear evidence of a coherent oscillation, but the fact that the same periodicity is observed in both the velocities and EWs supports this hypothesis. A much larger data set will be needed to confirm or reject the 47-min periodicity. Unfortunately, the time resolution of our 1.1-cycle long NTT data is insufficient to sample it properly.

### 5.6.3 Doppler tomography

The  $H\alpha$  Doppler map of V380 Oph is presented in Fig. 4. The  $H\alpha$  emission is mainly concentrated in the lower-left quadrant of the tomogram, around ( $V_x \sim -250, V_y \sim -100$ )  $\text{km s}^{-1}$ , a clear signature of the SW Sex stars.

### 5.6.4 SW Sex class membership

V380 Oph displays all the characteristic features described in Sect. 5.5.3 for AH Men. Therefore, it fully qualifies as a SW Sex star. Apart from that, the radial velocities and the EWs show rapid variations with a likely periodicity of 46.7 min, which can be related to the rotation of a magnetic white dwarf.

## 5.7 LQ Peg

LQ Peg (= PG 2133+115 = Peg 6) was found as a peculiar absorption-line object in the Palomar–Green survey (Green et al. 1986), and was classified as a CV of possible UX UMa type from follow-up optical and ultraviolet *IUE* spectroscopy (Ferguson, Green & Liebert 1984). Ringwald (1993) derived an uncertain orbital period of 2.9 h from radial velocity measurements. The optical spectrum of LQ Peg appears to be highly variable, switching from weak Balmer emission superimposed on broad absorptions to pure Balmer and  $\text{He II } \lambda 4686$  emission profiles (see the spectra shown in Ferguson et al. 1984 and Papadaki et al. 2006).

Photometrically, LQ Peg undergoes deep ( $\sim 3 - 4$  mag), VY Scl-like low states (Sokolov et al. 1996; Watanabe 1999; Kato & Uemura 1999; Honeycutt & Kafka 2004; Kafka & Honeycutt 2005), which drive the system down to  $V \sim 18$ . Additionally, time resolved photometric observations in both the high and low states show no coherent oscillations apart from strong flickering (Misselt & Shafter 1995;

Schmidtke et al. 2002). Papadaki et al. (2006) found a 2.99-h wave in the optical light curve spanning about 50 hours spread over three months. Whether this modulation is the actual orbital period or a positive (or negative) superhump has still to be investigated. There might also be a QPO at  $\sim 30$  min, but no firm conclusion could be addressed.

### 5.7.1 $H\alpha$ radial velocities, trailed spectrum, and Doppler tomogram

The average of all the spectra we obtained at the NTT (Fig. 1) shows very narrow  $H\alpha$  ( $\text{FWHM} \simeq 310 \text{ km s}^{-1}$ ) and  $\text{He I } \lambda 6678$  ( $\text{FWHM} \simeq 210 \text{ km s}^{-1}$ ) lines purely in emission, indicating a low orbital inclination. The  $H\alpha$  radial velocities were measured by applying the double-Gaussian method with a separation of  $200 \text{ km s}^{-1}$  and  $\text{FWHM} = 200 \text{ km s}^{-1}$ , which yielded the curve presented in Fig. 14. A sine fit to the velocities gives a period of 2.8 h (that is highly unreliable) and an amplitude of only  $\sim 12 \text{ km s}^{-1}$ .

The  $H\alpha$  trailed spectrum (Fig. 3) does not provide any useful information either, as expected from the small amplitude of the radial velocity curve. On the other hand, the  $H\alpha$  EWs do not show periodic rapid variations. In the  $H\alpha$  Doppler tomogram (Fig. 4), the lack of resolved structure in the line profiles translates into a single emission spot centred on the origin. It is therefore apparent that higher resolution spectroscopic data are needed to eventually obtain the actual orbital period. Until then no speculation about the nature of the photometric period should be made.

## 5.8 AHPic

AHPic (= EC 05565–5934) was identified as a CV in the Edinburgh–Cape Survey by Chen et al. (2001). They classified the system as a UX UMa-type star, based on several blue spectra which at one epoch showed the Balmer lines in weak and shallow absorption, while two years later they were present in weak emission. Chen et al. also performed time resolved photometry of the system and found a clear modulation at  $3.40 \pm 0.04$  h, which they proposed as the orbital period. In addition, the light curves also displayed rapid variations with a time-scale of 10 – 20 min

### 5.8.1 $H\alpha$ radial velocities and trailed spectrum

In our average spectrum (Fig. 1), the  $H\alpha$  line is clearly in emission, although a shallow broad absorption is also seen when the flux scale is properly adjusted. The  $H\alpha$  emission shows a single-peaked profile with  $\text{FWHM} \simeq 760 \text{ km s}^{-1}$ , typical for nova-likes viewed at intermediate to low inclination.

We measured the  $H\alpha$  radial velocities by applying the double-Gaussian technique ( $1200 \text{ km s}^{-1}$  separation,  $\text{FWHM} = 150 \text{ km s}^{-1}$ ). A sine fit provided an orbital period of  $P_{\text{orb}} = 0.146 \pm 0.04$  d. An initial  $H\alpha$  trailed spectrogram with relative orbital phases computed using the  $T_0$  from the radial velocity curve shows several emission S-waves. A close inspection of the individual profiles reveals a multi-component structure with a broad emission component giving rise to line wings extending up to  $\sim \pm 800 \text{ km s}^{-1}$ , and probably two other components moving closer to the

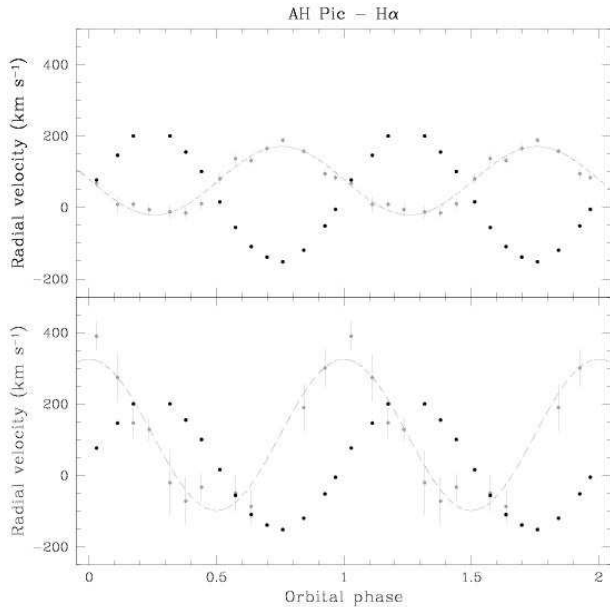


**Figure 15.** *Top:* the  $H\alpha$  radial velocity curve of AH Pic computed by cross-correlation with a double-Gaussian template (gray;  $1200 \text{ km s}^{-1}$  separation,  $\text{FWHM} = 150 \text{ km s}^{-1}$ ), and best sine fit (gray dashed curve). Black dots are the  $H\alpha$  radial velocity curve of the likely donor emission. A deviant point has been omitted. *Bottom:* the same but with a Gaussian separation of  $2000 \text{ km s}^{-1}$  (gray). A 0.25-orbital cycle delay with respect to the motion of the white dwarf is apparent. The orbital cycle has been plotted twice.

line core which produce double peaks with changing relative intensity. The component with smallest velocity amplitude has maximum intensity at  $\varphi_r \sim 0.5$ . This suggests a likely origin in the irradiated hemisphere of the donor star. In order to obtain absolute phases we isolated this component by applying the usual method and obtained  $T_0(\text{HJD}) = 2453478.547 \pm 0.001$  and  $K_{\text{irr}} = 184 \pm 3 \text{ km s}^{-1}$ .

With the aim of searching for phase offsets, we constructed a new radial velocity curve of  $H\alpha$  by using the double-Gaussian technique, but going further into the line wings ( $2000 \text{ km s}^{-1}$  separation,  $\text{FWHM} = 150 \text{ km s}^{-1}$ ). All the radial velocity curves are presented in Fig. 15. The wing velocities clearly lag the motion of the white dwarf by  $\sim 0.25$  orbital cycle, which is a clear indication of a SW Sex nature.

A new  $H\alpha$  trailed spectrum with absolute phases is shown in Fig. 3. There are two emission components clearly moving in counter phase. One is located at the central part of the line, which peaks at a velocity of  $\sim 180 \text{ km s}^{-1}$  at  $\varphi_a = 0.25$  (we have assumed an origin on the heated donor star), whilst the other is peaking at velocities of about  $300 \text{ km s}^{-1}$  at  $\varphi_a \simeq 0.8$ . A third, much broader emission S-wave is responsible for the extended wings up to  $\pm 800 \text{ km s}^{-1}$  and for the delayed velocities. Finally, the EWs of the  $H\alpha$  line have two minima, one at  $\varphi_a \simeq 0$  and a shallower one (likely filled by the maximum emission from the donor star) at  $\varphi_a \simeq 0.5$ . As in the case of HL Aqr, the trailed spectrum of AH Pic shows enhanced blueshifted absorption at  $\varphi_a \sim 0.4 - 0.5$ .

### 5.8.2 Doppler tomography

The  $H\alpha$  Doppler tomogram of AH Pic can be seen in Fig. 4. Two emission sites are clearly seen. One is located at the expected position of the donor star, and the other at ( $V_x \sim 0, V_y \sim +180$ )  $\text{km s}^{-1}$ . This is obvious, as the S-wave which produces this spot is assumed to come from the heated face of the secondary star. However, this assumption is supported by two observations: (i) the presence of another emission spot in the lower left quadrant of the Doppler map, and (ii) the 0.25-cycle phase delay seen in the radial velocity curve of the line wings. These are characteristic features of the SW Sex stars.

### 5.8.3 Orbital inclination

Proceeding in the same way as with other systems with apparent emission from the donor star already presented, we can place limits to the orbital inclination from estimates of the  $K$ -correction. For AH Pic we assume  $M_1 = 0.75 M_\odot$  and  $M_2 = 0.24 M_\odot$  and, therefore,  $q = 0.32$ . From a sine fit to the donor emission radial velocities we obtain  $K_{\text{irr}} = 184 \pm 3 \text{ km s}^{-1}$ . Hence, the radial velocity amplitude of the donor star ranges between  $207 < K_2 < 293 \text{ km s}^{-1}$ , and the orbital inclination between  $25^\circ < i < 37^\circ$ .

### 5.8.4 SW Sex class membership

Apart from the emission in the lower left quadrant of the tomogram mentioned above, AH Pic shows many other features typical of the SW Sex stars. The  $H\alpha$  emission has single-peaked profiles and shows a high-velocity S-wave. Contrary to the rule, this S-wave has its maximum blueshift at  $\varphi_a \sim 0.3$ , not at  $\sim 0.5$  as can be expected (the same phasing is observed in HL Aqr). Instead, there is blueshifted absorption at  $\varphi_a \sim 0.5$ , as in the case of HL Aqr. The similarities with HL Aqr are not unexpected, as the estimated orbital inclinations are very close. The deeper absorption seen in HL Aqr may therefore be a consequence of its lower inclination. Finally, the radial velocity curve measured in the line wings lags the motion of the white dwarf by 0.25 cycle. We conclude that AH Pic is very likely a SW Sex star.

## 5.9 V992 Sco

V992 Sco (Nova Scorpii 1992) was discovered as a possible nova in outburst by Camilleri (1992), and was spectroscopically confirmed by della Valle & Smette (1992). Although it was a slow nova, high-speed photometry performed 10 years after outburst showed that the nova had faded by about 10 mag and revealed a fundamental period of 0.154 d ( $= 3.686 \text{ h}$ , Woudt & Warner 2003). The inclination of the system was estimated as intermediate, probably  $\sim 40^\circ$ .

### 5.9.1 $H\alpha$ radial velocities and trailed spectrum

Our spectrum of V992 Sco (Fig. 1) was taken 13 years after the nova explosion. It shows a strong, multi-peaked  $H\alpha$  emission line. It is therefore apparent that even though the binary is dominating in the  $V$ -band light curve, the nova-shell is still the dominating  $H\alpha$  emission source. However, in order



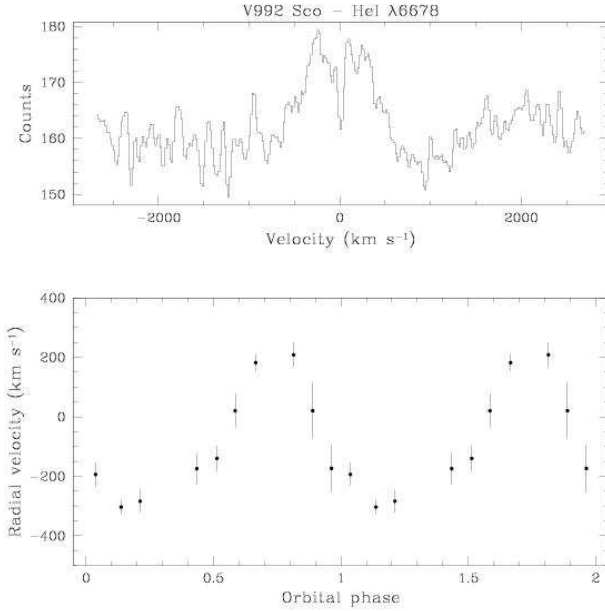


**Figure 16.** *Top panel:* the He I  $\lambda 6678$  average line profile of V992 Sco. Prior to averaging, the individual spectra were smoothed by using a 1 pixel (FWHM) Gaussian template. A double peak may be present. *Bottom panel:* the He I  $\lambda 6678$  radial velocity curve of V992 Sco computed by cross-correlation with a single Gaussian template (FWHM = 400 km s<sup>-1</sup>). Orbital phases are relative. A whole orbital cycle has been repeated for clarity.

to spectroscopically confirm Woudt & Warner’s orbital period we tried to find radial velocity variations in the much weaker He I  $\lambda 6678$  emission line (Fig. 16, top panel). The radial velocities were measured by cross-correlation with a single Gaussian template (FWHM = 400 km s<sup>-1</sup>). The period of the best fitting sine is 0.147 d, in agreement with the photometric result. The He I  $\lambda 6678$  radial velocities folded on Woudt & Warner’s period are shown in Fig. 16. Our results indicate that the nova shell, which dominates the H $\alpha$  emission, makes only a small contribution to He I  $\lambda 6678$ .

The H $\alpha$  trailed spectrum can be seen in Fig. 3. That of He I  $\lambda 6678$  has not been included because of its poor quality. The analysis of better signal-to-noise ratio He I  $\lambda 6678$  spectra can eventually provide an accurate orbital period for V992 Sco.

## 5.10 LN UMa

As many other nova-like CVs, LN UMa (= PG 1000+667 = UMa7) was found in the Palomar–Green survey (Green et al. 1986). The first spectroscopic analysis was carried out by Ringwald (1993), who first identified LN UMa as a nova-like showing narrow Balmer emission lines with a probable orbital period of 4.06 h. A more detailed spectroscopic study by Hillwig, Robertson & Honeycutt (1998) revealed a narrow (FWHM = 490 km s<sup>-1</sup>) H $\beta$  emission line superimposed on a much broader absorption. Their H $\beta$  radial velocity curve yielded an orbital period of  $0.1444 \pm 0.0001$  d (= 3.465  $\pm$  0.002 h). In addition, long term photometric monitoring (Hillwig et al. 1998; Honeycutt & Kafka 2004) showed LN UMa to be a VY Scl star which undergoes  $\sim$  3-mag fades from its usual brightness at  $V \simeq 15.0$ .

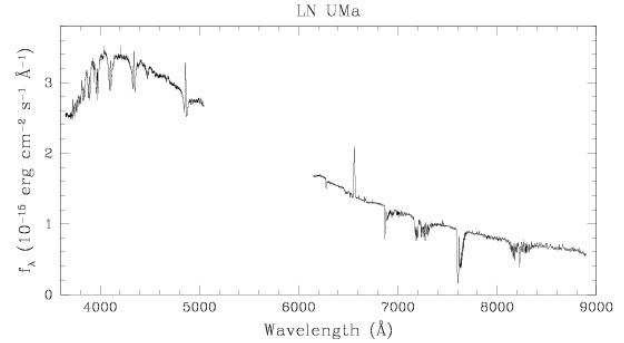


**Figure 17.** WHT flux-calibrated, average spectrum of LN UMa. No telluric absorption correction has been applied.

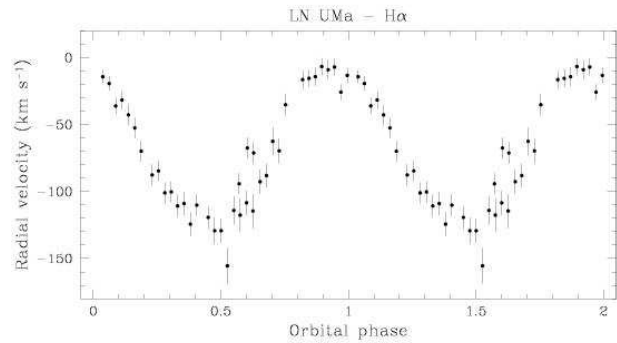


**Figure 18.** H $\alpha$  radial velocity curve of LN UMa computed by cross-correlation with a double-Gaussian template (800 km s<sup>-1</sup> separation, FWHM = 200 km s<sup>-1</sup>). The velocities lag the motion of the white dwarf by  $\sim$  0.2 cycle. A whole orbital cycle has been repeated for clarity.

### 5.10.1 H $\alpha$ radial velocities and trailed spectrum

Our average spectrum (Fig. 17) displays narrow, single-peaked emission lines of the Balmer series superimposed on broad absorptions, with the exception of H $\alpha$ . Very much weaker He I emission lines as well as He II  $\lambda 4686$  and the Bowen blend are also observed. The average H $\alpha$  emission profile (Fig. 1) has FWHM = 510 km s<sup>-1</sup> and EW = 6 Å. We constructed the radial velocity curve of the H $\alpha$  line by using the double-Gaussian method (FWHM = 200 km s<sup>-1</sup>) with a separation of 800 km s<sup>-1</sup>, which is presented in Fig. 18. A sine fit gives a period of  $0.1448 \pm 0.0008$  d, consistent with Hillwig et al.’s findings. We will adopt their  $P_{\text{orb}} = 0.1444$  d as they benefited from a longer spectroscopic data base.

A preliminary H $\alpha$  trailed spectrum with orbital phases calculated using the  $T_0$  from the above sine fit shows a high-velocity emission S-wave and a flux deficit close to the S-wave’s bluest excursion ( $\sim$  -700 km s<sup>-1</sup>). Similarly to other systems already discussed in this paper, this component reaches maximum blue velocity at  $\varphi_r \sim 0.25$  when using this phase convention. If SW Sex-related at all it should do at  $\varphi_a \sim 0.5$ , so we corrected the initial  $T_0$  accordingly. With the new  $T_0$  (Table 3), the radial velocity curve of the H $\alpha$  wings show a  $\Delta\varphi \sim 0.2$  delay with respect to the actual time of zero phase.

**Table 4.** Summary table of SW Sex classification.

System	Single peaks	High-velocity S-wave	0.5-absorption	Phase shift	Doppler	Line flaring	SW Sex?
HL Aqr	✓	✓ <sup>1</sup>	×	✓	✓	×	✓
BO Cet	✓	✓	✓	✓	✓	✓	✓
V849 Her	✓	×	×	×	×	×	×
V393 Hya	×	×	×	×	×	×	×
AH Men	✓	✓	✓	✓	✓	×	✓
V380 Oph	✓	✓	✓	✓	✓	✓	✓
LQ Peg	✓	×	×	×	×	×	×
AH Pic	✓	✓ <sup>1</sup>	×	✓	✓	×	✓
V992 Sco	—	—	—	—	—	—	—
LN UMa	✓	✓	✓	✓	×	×	✓

<sup>1</sup>) In absorption.<sup>2</sup>) Better spectral resolution needed.

### 5.10.2 Doppler tomography

The H $\alpha$  Doppler tomogram of LN UMa (Fig. 4) only shows an emission blob approximately centred on the origin. This, together with the small radial velocity amplitude observed  $\sim 60 \text{ km s}^{-1}$ , suggests the need for data with much better spectral resolution in order to resolve the emission features on a Doppler map.

### 5.10.3 SW Sex class membership

The H $\alpha$  emission line of LN UMa has a single-peaked profile throughout the whole orbit. It also shows a high-velocity S-wave with maximum blueshift at  $\varphi_a \sim 0.5$ , and displays an absorption component crossing the line core from red to blue at the same instant. Moreover, the H $\alpha$  line wings lag the expected instant of zero phase by  $\sim 0.2$  cycle. Alas, the spectral resolution prevented us from resolving the emission components on a Doppler tomogram. LN UMa is therefore classified as a new SW Sex star.

In Table 4 we summarise the SW Sex classification criteria for all the systems presented in this paper.

## 6 THE IMPACT OF SW SEX STARS ON THE NOVA-LIKE POPULATION

Remarkably, 60 per cent of the nova-likes presented in this paper are SW Sex stars, namely, HL Aqr, BO Cet, AH Men, V380 Oph, AHPic, and LN UMa. Spectroscopic data with better signal-to-noise ratio and/or better spectral resolution are needed to address any conclusion on the remaining three systems. Our findings increase the number of known SW Sex stars to 35 (see Rodríguez-Gil et al. 2007 for a list), 37 per cent of which are non-eclipsers. It is therefore increasingly clear that the old requirement for eclipses is actually due to a selection effect. Hence, scenarios which rely on a high inclination, like those invoking the 0.5-absorption caused by material in the L<sub>3</sub> point (Honeycutt et al. 1986), a disc-anchored magnetic propeller (Horne 1999), and self-obscuration of the inner disc by a flared outer disc (Knigge et al. 2000) have to be revised. In fact, as our results on HL Aqr show, the orbital inclination may play a fundamental role in the spectroscopic behaviour

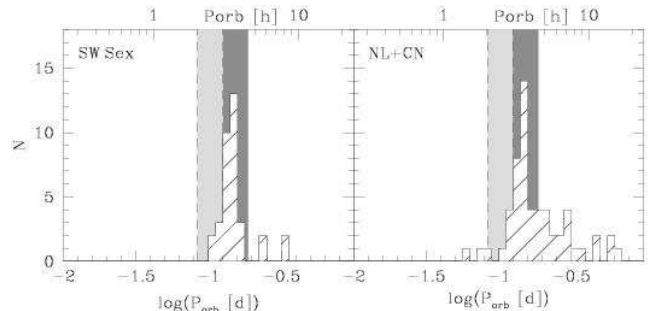


**Figure 19.** Period distributions of confirmed SW Sex stars (left panel) and nova-likes and classical novae that are not known to exhibit SW Sex behaviour so far.

of the SW Sex stars, with the lower inclination systems looking rather different than the higher inclination ones.

The orbital period distributions of the known SW Sex stars and the non-SW Sex nova-likes and classical novae are presented in Fig. 19. The latter was constructed from the Ritter (Ritter & Kolb 2003), CVcat (Kube et al. 2003), and Downes (Downes et al. 2005) catalogues, and only robust orbital period determinations were included. Remarkably, close to 40 per cent (35 out of 93) of the whole nova-like/classical nova population are SW Sex stars. Moreover, the impact of SW Sex stars on this population can reach 50 per cent if a number of SW Sex candidates are confirmed as members of the class. In the narrow  $\sim 3 - 4$  h orbital period range the situation is even more striking: almost *half* of the inhabitants are SW Sex stars (26 out of 53). This fraction is likely bound to increase as more SW Sex stars are found in this orbital period interval, as the similarity of the SW Sex period distribution with that of non-SW Sex nova-likes/classical novae—which also shows a spike in the  $\sim 3 - 4$  h range—suggests.

This pile-up of SW Sex stars is difficult to reconcile with the standard CV evolution theory. If the magnetic nature of these systems (Rodríguez-Gil et al. 2001; Hameury & Lasota 2002) is confirmed, then the majority of CVs close to the upper boundary of the period gap will be magnetic. This is clearly at odds with the majority of CVs below the gap being non-magnetic. On the other hand, Podsiadlowski et al. (2003) suggested that the population

of CVs longward of  $P_{\text{orb}} \simeq 4.7$  h is dominated by systems with evolved donors. A direct consequence of this is that the dominance of SW Sex stars among CVs with unevolved secondary stars above the gap would be even higher. Yet this is very speculative as no direct measurement of the stellar masses (i.e. a full dynamical solution for both masses) in any SW Sex star has been achieved so far, which is at the same time a weakness in the  $M_2 - P_{\text{orb}}$  sequence of Knigge (2006) as it lacks robust dynamical  $M_2$  determinations for the numerous SW Sex class. It is therefore apparent that the study of the increasing family of the SW Sex stars, with special emphasis on the determination of the stellar masses involved, is instrumental for the current theory of CV evolution (see Rodríguez-Gil et al. 2007, for a more detailed discussion).

## ACKNOWLEDGMENTS

We thank the anonymous referee for valuable comments. PRG thanks the European Southern Observatory for granting a stay within their Visiting Scientist programme. BTG was supported by a PPARC Advanced Fellowship. The use of the MOLLY, DOPPLER, and TRAILER packages developed by Tom Marsh is acknowledged. We also acknowledge the use of the Simbad database operated at CDS, Strasbourg, France. Based in part on observations collected at the European Southern Observatory, La Silla, Chile, and on observations made with the William Herschel Telescope, which is operated on the island of La Palma by the Isaac Newton Group in the Spanish Observatorio del Roque de los Muchachos of the Instituto de Astrofísica de Canarias (IAC).

## REFERENCES

- Aungwerojwit A., et al., 2005, *A&A*, 443, 995  
 Buckley D. A. H., Cropper M., Ramsay G., Wickramasinghe D. T., 1998, *MNRAS*, 299, 83  
 Buckley D. A. H., Warner B., Remillard R. A., Tuohy I. R., Sullivan D. J., 1993, *MNRAS*, 265, 926  
 Camilleri P., 1992, *IAU Circ.*, 5526, 1  
 Casares J., Martínez-Pais I. G., Marsh T. R., Charles P. A., Lázaro C., 1996, *MNRAS*, 278, 219  
 Chen A., O'Donoghue D., Stobie R. S., Kilkeny D., Warner B., 2001, *MNRAS*, 325, 89  
 Dall T. H., Schmidtobreick L., 2004, *Inf. Bull. Variable Stars*, 5567, 1  
 della Valle M., Smette A., 1992, *IAU Circ.*, 5529, 1  
 Dhillon V. S., Marsh T. R., Jones D. H. P., 1991, *MNRAS*, 252, 342  
 Downes R. A., Webbink R. F., Shara M. M., Ritter H., Kolb U., Duerbeck H. W., 2005, *VizieR Online Data Catalog*, 5123  
 Drew J. E., 1997, in Wickramasinghe D. T., Ferrario F., Bicknell G., eds, *ASP Conf. Ser. Vol. 121, Accretion Phenomena and Related Outflows*. Astron. Soc. Pac., San Francisco, p. 465  
 Eggleton P. P., 1983, *ApJ*, 268, 368  
 Ferguson D. H., Green R. F., Liebert J., 1984, *ApJ*, 287, 320  
 Gänsicke B. T., Koester D., 1999, *A&A*, 346, 151  
 Green R. F., Schmidt M., Liebert J., 1986, *ApJS*, 61, 305  
 Haefner R., Schoembs R., 1987, *MNRAS*, 224, 231  
 Hameury J. M., Lasota J. P., 2002, *A&A*, 394, 231  
 Haro G., Luyten W. J., 1962, *Boletín de los Observatorios Tonantzintla y Tacubaya*, 3, 37  
 Hellier C., 1996, *ApJ*, 471, 949  
 Hellier C., 2000, *New Astronomy Reviews*, 44, 131  
 Hellier C., Robinson E. L., 1994, *ApJ*, 431, L107  
 Hillwig T. C., Robertson J. W., Honeycutt R. K., 1998, *AJ*, 115, 2044  
 Hoard D. W., Szkody P., 1997, *ApJ*, 481, 433  
 Hoard D. W., Thorstensen J. R., Szkody P., 2000, *ApJ*, 537, 936  
 Honeycutt R. K., Kafka S., 2004, *AJ*, 128, 1279  
 Honeycutt R. K., Schlegel E. M., Kaitchuck R. H., 1986, *ApJ*, 302, 388  
 Horne K., 1986, *PASP*, 98, 609  
 Horne K., 1999, in Hellier C., Mukai K., eds, *ASP Conf. Ser. Vol. 157, Annapolis Workshop on Magnetic Cataclysmic Variables*. Astron. Soc. Pac., San Francisco, p. 349  
 Hunger K., Heber U., Koester D., 1985, *A&A*, 149, L4  
 Kafka S., Honeycutt R. K., 2004, *AJ*, 128, 2420  
 Kafka S., Honeycutt R. K., 2005, *Inf. Bull. Variable Stars*, 5597, 1  
 Kato T., Uemura M., 1999, *Inf. Bull. Variable Stars*, 4786, 1  
 Kilkeny D., O'Donoghue D., Koen C., Stobie R. S., Chen A., 1997, *MNRAS*, 287, 867  
 Knigge C., 2006, *MNRAS*, in press (astro-ph/0609671)  
 Knigge C., Long K. S., Hoard D. W., Szkody P., Dhillon V. S., 2000, *ApJ*, 539, L49  
 Kube J., Gänsicke B. T., Euchner F., Hoffmann B., 2003, *A&A*, 404, 1159  
 Marsh T. R., Duck S. R., 1996, *New Astronomy*, 1, 97  
 Marsh T. R., Horne K., 1988, *MNRAS*, 235, 269  
 Martínez-Pais I. G., de la Cruz Rodríguez J., Rodríguez-Gil P., 2007, *MNRAS*, submitted  
 Misselt K. A., Shafter A. W., 1995, *AJ*, 109, 1757  
 Mouchet M., Siess L., Drew J., Lasota J. P., Buckley D. A. H., Bonnet-Bidaud J. M., 1996, *A&A*, 306, 212  
 Muñoz-Darias T., Casares J., Martínez-Pais I. G., 2005, *ApJ*, 635, 502  
 Munari U., Zwitter T., 1998, *A&AS*, 128, 277  
 Papadaki C., Boffin H. M. J., Sterken C., Stanishev V., Cuypers J., Boumis P., Akras S., Alikakos J., 2006, *A&A*, 456, 599  
 Patterson J., 1995, *PASP*, 107, 657  
 Patterson J., et al., 2002, *PASP*, 114, 1364  
 Patterson J., et al., 2005, *PASP*, 117, 1204  
 Podsiadlowski P., Han Z., Rappaport S., 2003, *MNRAS*, 340, 1214  
 Prinja R. K., Drew J. E., Rosen S. R., 1992, *MNRAS*, 256, 219  
 Ringwald F. A., 1993, PhD thesis, Dartmouth College  
 Ritter H., Kolb U., 2003, *A&A*, 404, 301  
 Rodríguez-Gil P., 2005, in Hameury J.-M., Lasota J.-P., eds, *ASP Conf. Ser. Vol. 330, The Astrophysics of Cataclysmic Variables and Related Objects*. Astron. Soc. Pac., San Francisco, p. 335  
 Rodríguez-Gil P., Casares J., Martínez-Pais I. G., Hakala P., Steeghs D., 2001, *ApJ*, 548, L49

- Rodríguez-Gil P., Gänsicke B. T., Araujo-Betancor S., Casares J., 2004, MNRAS, 349, 367
- Rodríguez-Gil P., Gänsicke B. T., Barwig H., Hagen H.-J., Engels D., 2004, A&A, 424, 647
- Rodríguez-Gil P., et al., 2005, A&A, 440, 701
- Rodríguez-Gil P., Martínez-Pais I. G., 2002, MNRAS, 337, 209
- Rodríguez-Gil P., Martínez-Pais I. G., Casares J., Villada M., van Zyl L., 2001, MNRAS, 328, 903
- Rodríguez-Gil P et al., 2007, MNRAS, submitted
- Scargle J. D., 1982, ApJ, 263, 835
- Schmidtke P. C., Ciudin G. A., Indlekofer U. R., Johnson D. R., Fried R. E., Honeycutt R. K., 2002, in Gänsicke B. T., Beuermann K., Reinsch K., eds, ASP Conf. Ser. Vol. 261, The Physics of Cataclysmic Variables and Related Objects. Astron. Soc. Pac., San Francisco, p. 539
- Schneider D. P., Young P., 1980, ApJ, 238, 946
- Sefako R. R., Glass I. S., Kilkenny D., de Jager O. C., Stobie R. S., O'Donoghue D., Koen C., 1999, MNRAS, 309, 1043
- Shafter A. W., 1985, AJ, 90, 643
- Shugarov S. Y., Katysheva N. A., Seregina T. M., Volkov I. M., 2005, in Hameury J.-M., Lasota J.-P., eds, ASP Conf. Ser. Vol. 330, The Astrophysics of Cataclysmic Variables and Related Objects. Astron. Soc. Pac., San Francisco, p. 495
- Smith D. A., Dhillon V. S., Marsh T. R., 1998, MNRAS, 296, 465
- Sokolov D. A., Shugarov S. Y., Pavlenko E. P., 1996, in Evans A., Wood J. H., eds, Proc. IAU Coll. 158, Cataclysmic Variables and Related Objects. Kluwer Academic Publishers, Dordrecht, p. 219
- Stanishev V., Kraicheva Z., Boffin H. M. J., Genkov V., 2002, A&A, 394, 625
- Steehgs D., 2003, MNRAS, 344, 448
- Szkody P., Piché F., 1990, ApJ, 361, 235
- Thorstensen J. R., Davis M. K., Ringwald F. A., 1991, AJ, 102, 683
- Thorstensen J. R., Ringwald F. A., Wade R. A., Schmidt G. D., Norworthy J. E., 1991, AJ, 102, 272
- Thorstensen J. R., Taylor C., 2000, MNRAS, 312, 629
- Thorstensen J. R., Taylor C. J., 2001, MNRAS, 326, 1235
- Warner B., 2004, PASP, 116, 115
- Warner B., Wickramasinghe D. T., 1991, MNRAS, 248, 370
- Watanabe T., 1999, VSOLJ Variable Star Bull., 34, 3
- Wetherick D. K., Prinja R. K., Howell S. B., Wagner R. M., 2003, MNRAS, 346, 861
- Woudt P. A., Warner B., 2003, MNRAS, 340, 1011
- Wu K., Wickramasinghe D. T., 1991, MNRAS, 252, 386
- Young P., Schneider D. P., Shectman S. A., 1981, ApJ, 245, 1035
- Zwitter T., Munari U., 1995, A&AS, 114, 575